Stereoselective glucuronidation metabolism, pharmacokinetics, anti-amnesic pharmacodynamics, and toxic properties of vasicine enantiomers in vitro and in vivo

Yudan Zhu, Wei Liu, Shenglan Qi, Hanxue Wang, Yuwen Wang, Gang Deng, Yunpeng Zhang, Shuping Li, Chao Ma, Yongli Wang, Xuemei Cheng, Changhong Wang

PII: S0928-0987(18)30362-2
DOI: doi:10.1016/j.ejps.2018.07.058
Reference: PHASCI 4634

To appear in: *European Journal of Pharmaceutical Sciences*

Received date: 19 February 2018
Revised date: 24 July 2018
Accepted date: 30 July 2018

Please cite this article as: Yudan Zhu, Wei Liu, Shenglan Qi, Hanxue Wang, Yuwen Wang, Gang Deng, Yunpeng Zhang, Shuping Li, Chao Ma, Yongli Wang, Xuemei Cheng, Changhong Wang , Stereoselective glucuronidation metabolism, pharmacokinetics, anti-amnesic pharmacodynamics, and toxic properties of vasicine enantiomers in vitro and in vivo. Phasci (2018), doi:10.1016/j.ejps.2018.07.058

Stereoselective Glucuronidation Metabolism, Pharmacokinetics, Anti-Amnesic Pharmacodynamics, and Toxic Properties of Vasicine Enantiomers *in vitro* and *in vivo*

Yudan Zhu [a, 1], Wei Liu [a, 1], Shenglan Qi [a], Hanxue Wang [a], Yuwen Wang [a], Gang Deng [a], Yunpeng Zhang [a], Shuping Li [a], Chao Ma [a], Yongli Wang [a, b], Xuemei Cheng [a,b], Changhong Wang [a, b] *

[a]*Institute of Chinese Materia Medica, Shanghai University of Traditional Chinese Medicine; The MOE Key Laboratory for Standardization of Chinese Medicines and The SATCM Key Laboratory for New Resources and Quality Evaluation of Chinese Medicines, 1200 Cailun Rood, Shanghai 201203, China*

[b]*Shanghai R&D Centre for Standardization of Chinese Medicines, 1200 Cailun Rood, Shanghai 201203, China*

*Correspondence to: Professor Changhong Wang, Institute of Chinese Materia Medica, Shanghai University of Traditional Chinese Medicine, Shanghai 201203, China. Tel: 086-021-51322511, Fax: 086-021-51322519, E-mail: wchcxm@shutcm.edu.cn; wchcxm@hotmail.com (C.H. Wang)

[1]Yudan Zhu and Wei Liu contributed equally to this work.

Keywords: Vasicine enantiomers; Anti-amnesic; Glucuronidation; Pharmacokinetics; Stereoselective

Abstract

Vasicine (VAS) is a potential natural cholinesterase inhibitor for treatment of Alzheimer's disease. Due to one chiral centre (C-3) presenting in molecule, VAS has two enantiomers, *d*-vasicine (*d*-VAS) and *l*-vasicine (*l*-VAS). The study was undertaken to investigate the stereoselective glucuronidation metabolism, pharmacokinetics, anti-amnesic effect and acute toxicity of VAS enantiomers. In results, the glucuronidation metabolic rate of *l*-VAS was faster than *d*-VAS in human liver microsomes and isoenzymes tests, and it was proved that the UDP-glucuronosyltransferase (UGT) 1A9 and UGT2B15 were the major metabolic enzymes for glucuronidation of *l*-VAS, while only UGT1A9 for *d*-VAS, which take responsibility of the significantly less metabolic affinity of *d*-VAS than *l*-VAS in HLM and rhUGT1A9. The plasma exposure of *d*-VAS in rats was 1.3-fold and 1.6-fold higher than that of *l*-VAS after intravenous and oral administration of d-VAS and l-VAS, respectively. And the plasma exposure of the major glucuronidation metabolite *d*-VASG was one of tenth of *l*-VASG or more less, no matter by intravenous or oral administration. Both *d*-VAS and *l*-VAS were exhibited promising acetylcholinesterase (AChE) and butyrylcholinesterase (BChE) inhibitory activities, and the BChE inhibitory activity of *d*-VAS with IC_{50} of 0.03 ± 0.001 μM was significantly stronger than that of *l*-VAS with IC_{50} of 0.98 ± 0.19 μM. The molecular docking results indicated that *d*-VAS and *l*-VAS could bind to the catalytic active site (CAS position) either of human AChE and BChE, and the BChE combing ability of *d*-VAS (the score of GBI/WAS dG -7.398) was stronger than that of *l*-VAS (the score of GBI/WAS dG -7.135). Both *d*-VAS and *l*-VAS could improving the learning and memory on scopolamine-induced memory deficits in mice. The content of acetylcholine (ACh) after oral administration *d*-VAS increased more than that of *l*-VAS in mice cortex, through inhibiting cholinesterase (ChE) and increasing choline acetyltransferase (ChAT). In addition, the LD_{50} value of *d*-VAS (282.51 $mg \cdot kg^{-1}$) was slight lower than *l*-VAS (319.75 $mg \cdot kg^{-1}$). These results indicated that VAS enantiomers displayed significantly stereoselective metabolic, pharmacokinetics, anti-amnesic effect and toxic properties *in vitro* and *in vivo*. The *d*-VAS might be the dominant configuration for treating Alzheimer's disease.

1. Introduction

Chiral drugs exhibit distinct biochemical and pharmacological behaviors in the body, and the preclinical evaluation of an enantiomer must be carried out to develop chiral drugs containing at least one chiral centre and produce 2^{n-1} pairs of enantiomers (Shen et al., 2013). Widely used chiral drugs, such as amlodipine (antihypertensive), methylphenidate (stimulant) and salbutamol (antihasthma), play important roles in the treatment of some human diseases (Maddi et al., 2010; Bartl et al., 2017; Jacobson et al., 2017). The physiochemical and biochemical properties of racemic mixtures and individual stereoisomers might be different, and the affinity of enantiomers with target molecules (enzymes, receptors and transporters) might also be different, it would result in dissimilar pharmacodynamics and pharmacokinetics. In some cases, one enantiomer may have a desired beneficial effect, whereas others may produce deleterious side-effects or toxicity (Smith, 2009). Thus, the U.S. Food and Drug Administration (FDA), China State Food and Drug Administration (SFDA) and some departments in other countries have agreed that the pharmacological, pharmacokinetic and toxicological evaluation of individual enantiomer of each developing chiral drug must be quantified (FDA, 1992; SFDA, 2007).

Vasicine (VAS), a pyrrolo [2,1-b] quinazoline type alkaloid, has a chiral centre in C-3 and two enantiomers, namely *d*-vasicine (*d*-VAS) and *l*-vasicine (*l*-VAS) (the chemical structures were shown in Fig. S1) (Joshi et al., 1996). VAS was first isolated in 1924 from *Adhatoda vasica* (Acanthaceae), and most of the work on this molecule was conducted between the 1960s and 1990s. VAS has diverse pharmacologic actions, such as bronchodilatory (Mahindroo et al., 2005), antitussive (Liu et al., 2015a), abortifacient (Chandokhe, 1987), antimicrobial (Pa and Mathew, 2012), anti-inflammatory and antioxidant effects (Srinivasarao et al., 2006). In recent years, as a potential natural cholinesterase (ChE) inhibitor, VAS has exhibited promising anticholinesterase activity in preclinical models and has been studied in the development of treatments for Alzheimer's disease (AD) (Ali et al., 2016; Li et al., 2017; Liu et al., 2016; Zhao et al., 2013). Liu and colleagues suggested that VAS showed strong inhibition of acetylcholinesterase (AChE) and butyrylcholinesterase (BChE) activities with IC_{50} of 3.24 ± 0.08 μM and 0.1 ± 0.0 μM, respectively (Liu et al., 2014). Moreover, the *in vivo* pharmacokinetic study of VAS was found that the oral absolute bioavailability (*F*) of VAS was approximately 54.56% ± 7.33% with a short half-life of 1.5 h in rats (Liu et al., 2015b). VAS could be metabolized and converted into

vasicinone (VAO), 1,2,3,9-tetrahydropyrrolo [2,1-b] quinazolin-3-b-D-glucuronide (VASG), 1,2,3,9-tetrahydropyrrolo [2,1-b] quinazolin-3-ylhydrogen sulfate (VASS) and 9-oxo-1,2,3,9-tetrahydropyrrolo [2,1-b] quinazolin-3-b-D-glucuronide (VAOG) in rat *in vivo* (Liu et al., 2015c). Notably, the exposure level of VAS and its glucuronidation metabolite (VASG) in rat plasma is comparable, whether by oral or intravenous administration (Liu et al., 2015b; Liu et al., 2015c), and VAS and VASG were cumulatively excreted 29.9 ± 3.78% and 41.0 ± 6.92% from urine and feces within 72 hours after oral administration 45 mg/kg of *Rac*-VAS, respectively (Liu et al., 2016), implying that the glucuronidation of VAS is one of the most important metabolic pathway in rats. In addition, most metabolites maintain potential inhibitory activity against AChE and BChE, although it is weaker than that of VAS. These results implied that VAS undergoes a metabolic inactivation process *in vivo* with respect to cholinesterase inhibitory activity (Liu et al., 2015c). Although many studies have been conducted on VAS, the stereoselective properties of VAS enantiomers with respect to metabolism, pharmacokinetics, pharmacodynamics and toxicity were rarely studied.

The aim of the present study is to investigate the stereoselective metabolism, pharmacokinetics, anti-amnesic effects, and acute toxicity of *d*-VAS and *l*-VAS and provide valuable scientific research data for the discovery of novel anti-amnesic drugs from VAS enantiomers. The stereoselective pharmacokinetics and glucuronidation metabolic diversities of *d*-VAS and *l*-VAS were carried out in rats and in human liver microsomes (HLMs), pre-clinical animal liver microsomes and UDP-glucuronosyltransferase (UGT) isoenzymes. The *in vitro* anticholinesterase activity assay and molecular docking assay were performed and scopolamine-induced memory deficit mouse model were used to evaluate the stereoselective anti-amnesic effects of *d*-VAS and *l*-VAS. The toxic properties of VAS enantiomers were evaluated by acute toxicity tests.

2. Materials and methods

2.1. Chemicals and reagents

Racemic VAS (*rac*-VAS) and VAO were isolated from *Peganum harmala* L., and racemic VASS, VAOS, and VASG (purity> 98%) were obtained from rat urine samples after the oral administration of VAS in our laboratory (Liu et al., 2015b). They were identified using NMR (Bruker NMR AV 400, Bruker Bio Spin GmbH, Rheinstetten, Germany) and mass spectrometry data with purity of more than 98% and assayed through peak area normalization via HPLC. Pseudoephedrine hydrochloride (PSH)

was provided by the National Institute for the Control of Pharmaceutical and Biological Products (Beijing, China). Choline acetyltransferase (ChAT) assay kit was purchased from Nanjing Jiancheng Bioengineering Institute (No. A079-1, Nanjing, China). BChE from equine serum, AChE from *Electrophorus electricus*, chlormequat chloride, butyrocholine chloride (BCh), acetylcholine chloride (ACh), choline chloride (Ch), alamethicin, glucose 6-phosphate, glucose-6-phosphate dehydrogenase, nicotinamide adenine dinucleotide phosphate (NADPH), uridine diphosphate glucuronic acid (UDPGA), tris base, fluconazole, phenylbutazone, hecogenin, niflumic acid, and diclofenac were obtained from Sigma Aldrich Co. (St. Louis, MO, USA). Recombinant human UGT1A1, 1A3, 1A4, 1A6, 1A7, 1A8, 1A9, 1A10, 2B4, 2B7, 2B15, 2B17 (5 $mg \cdot mL^{-1}$) and pooled HLM (20 $mg \cdot mL^{-1}$, 32 donor pool; equal number of males and females) were purchased from BD Biosciences (San Jose, CA, USA). The liver microsomes of rats, mice, pigs, guinea pigs, dogs, monkeys, rabbits, bulls, sheep and camels were prepared using the reported method in our laboratory (Li et al., 2016). MCI Gel CHP 20P was purchased from Mitsubishi Chemical Corporation (Tokyo, Japan). Silica Gel C18 (MB 100-40/75) was purchased from Fuji Silysia Chemical Ltd. (Kasugai, Japan). HPLC grade acetonitrile and methanol were purchased from Fisher Scientific Co. (Santa Clara, USA). Formic acid of HPLC grade was purchased from Tedia Co. (Fairfield, USA). HPLC grade water was obtained by a Milli-Q Academic System (Millipore, Billerica, MA). The ACQUITY UPLC^{TM} HSS T3 column (100 mm × 2.1 mm, 1.8 μm) was purchased from Waters Corp. (MA, USA). All other reagents and solvents were of analytical grade.

2.2. Animals

Male C57BL/6 mice aged 6 weeks and guinea pigs (body weight 200–250 g) were obtained from the Animal Research Centre of Shanghai University of Traditional Chinese Medicine (Shanghai, China).Male and female Kunming mice (body weight, 18–22 g) and Sprague-Dawley rats (body weight, 180–200 g) were obtained from Shanghai Slac Laboratory Animal Co. Ltd. (Shanghai, China). All the animals were raised under controlled conditions at a temperature of 25 ± 2°C and 12 h light–dark cycle with free access to food and water for at least 7 days before the experiment. All the experiments performed on the animals were in accordance with the P.R. China legislation on the use and care of laboratory animals and approved by the Animal Care and Use Committee of Shanghai University of Traditional Chinese Medicine (Approval Number: ACSHU-2011-G115).

2.3. In vitro metabolic diversity of rac-VAS, d-VAS and l-VAS in human liver microsomes

2.3.1. Elimination of rac-VAS and its enantiomers in human liver microsomes

The elimination rates of *rac*-VAS and its enantiomers in HLM were determined. The entire incubation volume was 100 μL and contained HLM (0.5 mg protein·mL^{-1}) and alamethicin (50 μg·mg^{-1} protein) in 100 mM Tris-HCl buffer (pH 7.4). The solution with HLM and alamethicin was incubated 5 min at 37°C with shaking in advance. Subsequently, 10 mM glucose 6-phosphate, 4 mM magnesium chloride, 1 unit·mL^{-1}of glucose-6-phosphate dehydrogenase and 1 μM *rac*-VAS, *d*-VAS or *l*-VAS were added in the incubation system successively. The incubation reaction was initiated by the addition of 1 mM $NADP^+$ and 5 mM UDPGA (Nishimuta et al., 2011). The reaction process was terminated with 500 μL of ice-cold acetonitrile containing IS after incubation for 0, 10, 20, 40, 60, and 80 min, respectively. The mixture was centrifuged at 12000 × *g* for 10 min, and 540 μL of supernatant was evaporated to dryness by a gentle stream of nitrogen (37°C). The residue was dissolved by 90 μL of 5% methanol and centrifuged at 12000 × *g* for 10 min. The supernatant (5 μL) was injected for UPLC-MS/MS analysis. Data was processed through the GraphPad Prism 5.0, the concentration of the prototype VAS before the incubation start (0 min) is considered as 100%, and the remaining prototype concentration remaining at the remaining time points is converted to the remaining %. Then, the natural logarithm and incubation time of all remaining quantities were made into regression curves, and the slope K was obtained. The intrinsic clearance (CL_{int}) of *rac*-VAS and its enantiomers were estimated from the *in vitro* half-life of substrate depletion ($t_{1/2}$ = -0.693/k), incubation volume (V) and concentration of microsomal proteins in the incubation mixture (P) according to the following equation: $CL_{int} = (0.693/t_{1/2}) \times (V/P)$ (Obach et al., 1997).

2.3.2. Formation rates of glucuronide metabolites in pooled HLMs and pre-clinical animal liver microsomes

The formation rates of glucuronide metabolites in pooled HLM and pre-clinical liver microsomes (MoLM, monkey liver microsomes; CLM, camel liver microsomes; BLM, bull liver microsomes; SLM, sheep liver microsomes; DLM, dog liver microsomes; GLM, guinea pig liver microsomes; RLM, rat liver microsomes; MLM, mouse liver microsomes; PLM, pig liver microsomes; and RaLM, rabbit liver microsomes) were evaluated. The entire incubation volume was 100 μL and contained pooled HLM or pre-clinical animal liver microsomes (0.5 mg protein·mL^{-1}) and alamethicin (50 μg·mg^{-1} protein) in 100

mM Tris-HCl buffer (pH 7.4). The solution with HLM or pre-clinical liver microsomes and alamethicin were incubated 5 min at 37°C with shaking in advance. Subsequently, 10 mM glucose 6-phosphate, 4 mM magnesium chloride, 1 unit·mL^{-1}of glucose-6-phosphate dehydrogenase and 0.5 mM *rac*-VAS, *d*-VAS or *l*-VAS were added in the incubation system successively. Finally, the incubation reaction was initiated by the addition of 1 mM $NADP^+$ and 5 mM UDPGA (Nishimuta et al., 2011). The 100 μL mixed solution was incubated for 60 min at 37°C, 500 μL of ice-cold acetonitrile mixed with 5 ng·mL^{-1} IS (PSH) was added to immediately terminate the reactions. The mixture was then centrifuged at 12000 × *g* for 10 min, and 540 μL of the supernatant was evaporated to dryness by a gentle stream of nitrogen (37°C). The residue was dissolved in 90 μL of 5% methanol and centrifuged at 12000 × *g* for 10 min, and 5 μL of the supernatant was injected for UPLC-MS/MS analysis. Control samples without $NADP^+$, UDPGA or substrates were prepared. Each of incubation reaction was performed in three replicates.

2.3.3. Effect of UGT inhibitors on production rates of glucuronide metabolites in pooled HLM

In the effect of UGT inhibitors assay, *rac*-VAS and its enantiomers were incubated with pooled HLM (0.5 mg protein·mL^{-1}) and specific chemical inhibitors in the UDPGA-regenerating system. The incubation system (100 μL) contained the pooled HLM (0.5 mg protein·mL^{-1}), alamethicin (50 μg·mg^{-1} protein), *rac*-VAS or its enantiomers (250 μM), 4 mM magnesium chloride, Tris-HCl buffer (pH 7.4) and 5 mM UDPGA. The mixture was incubated at 37°C for 60 min, and the reaction was terminated by the addition of 500 μL of ice-cold acetonitrile containing IS (5 ng·mL^{-1} PSH). The selective inhibitors used were atazanavir (UGT1A1, IC_{50} 2.4 μM) (Zhang et al., 2005), hecogenin (UGT1A4, IC_{50} 1.5 μM) (Uchaipichat et al., 2006) and fluconazole (UGT2B7, IC_{50} 2.5 μM) (Raungrut et al., 2010) at individual concentrations of 1, 10 and100 μM; niflumic acid (UGT1A9, IC_{50} 25 μM) (Miners et al., 2011) at concentrations of 10, 100 and 500 μM; phenylbutazone (UGT1As, IC_{50} 500 μM) (Ballard et al., 2016) and diclofenac (UGT2B15, IC_{50} 500 μM) (Uchaipichat et al., 2004) at concentrations of 100, 500 and 1000 μM. The other operations were similar to the formation rates of glucuronide metabolites in pooled HLM. The control samples without inhibitors were prepared. Each of incubation was performed in three replicates. The percent inhibition was calculated as the formation rate of VASG in the inhibited samples ($V_{inhibited}$) relative to the formation rate of VASG in the control samples ($V_{control}$) according to the following equation: Percent inhibition=$(1-V_{inhibited}/V_{control}) \times 100\%$ (n=3).

2.3.4. Identification of rhUGT isoforms in human recombinant UGT systems

In the human recombinant UGTs assay, *rac*-VAS and its enantiomers were incubated with 12 human rhUGT enzymes (rhUGT 1A1, 1A3, 1A4, 1A6, 1A7, 1A8, 1A9, 2B4, 2B7, 2B10, 2B15 and 2B17). The incubation system (100 μL) contained the rhUGT enzymes (0.5 mg·mL^{-1}), alamethicin (50 μg·mg^{-1} protein), *rac*-VAS or its enantiomers (250 μM), 4 mM magnesium chloride, Tris-HCl buffer (pH 7.4) and 5 mM UDPGA. The mixture was incubated at 37°C for 60 min, and the reaction was terminated by the addition of 500 μL of ice-cold acetonitrile containing IS (5 ng·mL^{-1} PSH). The other operations were similar to the formation rates of glucuronide metabolites in pooled HLM. The control samples without human UGTs or substrates were prepared. Each of incubation reaction was performed in three replicates.

2.3.5. Glucuronidation kinetics in human recombinant UGT1A9 and UGT2B15 systems

The standard incubation mixtures contained *d*-VAS and *l*-VAS (15–250 μM) or *rac*-VAS (30–500 μM) and HLM (0.5 mg of protein·mL^{-1}) or rhUGT1A9 (0.5 mg of protein·mL^{-1}) and rhUGT2B15 (0.5 mg of protein·mL^{-1}). The procedures for the incubation were performed according to the protocols used in the recombinant human UGT enzymes. Each of incubation reaction was performed in three replicates. The supernatants were analysed by UPLC-MS/MS. The glucuronidation metabolite (*d*-VASG and *l*-VASG) formation rates of the VAS enantiomers were plotted against the concentrations of *d*-VAS and *l*-VAS to obtain the Michaelis-Menten constant (K_m) and maximum velocity (V_{max}) values of the reactions ($V = [V_{max1} \times S/(K_{m1} + S)] + [V_{max2} \times S/(K_{m2} + S)]$), [S] is the substrate concentration. This procedure was performed on Prism software (GraphPad Software Inc., San Diego, CA). All the results were expressed as mean ± standard error.

2.4. In vivo stereoselective pharmacokinetics of d-VAS and l-VAS in rats

2.4.1. Dose administration and pharmacokinetics

Thirty-two Sprague-Dawley rats were equally divided into four groups, two were intravenous dosage groups (1 mg·kg^{-1} of *d*-VAS and *l*-VAS, respectively) and two were oral dosage groups (7.5 mg·kg^{-1} of *d*-VAS and *l*-VAS, respectively). Approximately 0.25 mL of venous blood was collected from the angular vein of each rat at the following time points: 0, 2, 5, 15, 30, 45, 60, 120, 240, 480 and 720 min after intravenously and orally administration. The blood samples were centrifuged at 5000 × *g* at 4°C for 10 min to separate the plasma, which was then stored at –20°C until UPLC/MS/MS analysis.

2.4.2. Preparation of plasma samples and UPLC-MS/MS analysis

Aliquots of 100 μL of plasma samples were added with 50 μL of standard work solutions of PSH (IS) and 250 μL of acetonitrile in tubes to precipitate the protein. The mixture was vortex-mixed for 1 min and then centrifuged at 12000 × *g* for 10 min. Aliquots of 320 μL of the supernatant were transferred to another clean tube and dried by a gentle stream of nitrogen (37°C). Initial mobile phase (80 μL) was then added, and the mixture was vortexed for 1 min. An aliquot of 5 μL was injected into the UPLC-MS/MS system with a ACQUITY UPLC^{TM} HSS T3 column (2.1 mm × 100 mm, 1.8 mm, MA, USA) for analysis according to a previous protocol (Liu et al., 2015c) with minor modifications and partial verification for the VASG enantiomer assay (see Supplementary Table S1).

2.5. Anticholinesterase activity of d-VAS and l-VAS in vitro

The anticholinesterase activities of *l*-VAS, *d*-VAS, and 11 mixture samples with different ratios of *l*-VAS and *d*-VAS (*l*-VAS/*d*-VAS: 10:1, 8:1, 6:1, 4:1, 2:1, 1:1, 1:2, 1:4, 1:6, 1:8, 1:10) were performed as previously described, in which the ACh and BCh were used as substrates to determine the inhibitory activities against AChE and BChE, respectively (Liu et al., 2014). All the test mixtures were dissolved in 0.2% DMSO to obtain 20 mM solutions. Thereafter, a 100 μL incubation system containing 10 μL of the test compound solution and 40 μL of the enzyme solutions (with final concentrations: of 0.0035 unit·mL^{-1} for AChE, or 0.008 unit·mL^{-1} for BChE) were mixed and pre-incubated for 15 min at 25°C. Then, 50 μL of the substrate solution (final concentrations 5.50 μM for ACh or 7.15 μM for BCh) was added, and the resulting mixture was incubated for 20 min at 25°C. The reaction was terminated immediately by adding 300 μL of ice-cold acetonitrile solution (0°C), which was dissolved with 1.899 μM IS (chlormequat chloride). The mixed solution was then centrifuged (15000 × *g*, 10 min), and the supernatant was used for the UPLC-MS/MS analysis. The IC_{50} values of the VAS mixtures on AChE and BChE were calculated using the Prism software (GraphPad Software Inc., San Diego, CA, USA).

2.6. Molecular docking of d-VAS and l-VAS with human AChE and BChE

For the comparison between *d*-VAS and *l*-VAS with human AChE and BChE (hAChE and hBChE), in respect to interactions and bonds, antagonist-bound human ChE [Protein Data Bank code: 4BDT] was selected as the template of hAChE and hBChE (Nachon et al., 2013). The conformations of VAS enantiomers were searched in the MMFF94X force field of MOE. The best model generated and sorted

by GBVI/WSA dG score was energy minimized, and hydrogen ions were added using Protonate 3D in MOE. The final model was subjected to binding site analysis and docking study.

2.7. Anti-amnesic effect of rac-VAS, d-VAS, and l-VAS on scopolamine-induced memory deficits in mice

2.7.1. Morris water maze test of rac-VAS, d-VAS, and l-VAS

The detailed procedure of Morris water maze (MWM) test was conducted according to a previously described method (He et al., 2015). A total of 48 male C57BL/6 mice were randomly divided into six groups (eight mice per group), namely vehicle-treated group, scopolamine-treated group (1 $mg \cdot kg^{-1}$), donepezil-treated group (3 $mg \cdot kg^{-1}$), *d*-VAS-treated group (15 $mg \cdot kg^{-1}$), *l*-VAS-treated group (15 $mg \cdot kg^{-1}$), and *rac*-VAS-treated group (15 $mg \cdot kg^{-1}$). Donepezil, *rac*-VAS, *d*-VAS and *l*-VAS were administered by oral *gavage* 1 week prior to the behavioural testing. During the tests, donepezil, *rac*-VAS, *d*-VAS, and *l*-VAS were administered 1 h before the trial, and scopolamine was intraperitoneally (i.p.) injected 30 min after.

2.7.2. Collection of brain tissues

After the end of the MWM test, all mice were anaesthetized and decapitated, and their brains were removed rapidly on ice. The entire cerebral cortex and hippocampus of each brain tissue were isolated on ice and then immediately snap-frozen by liquid nitrogen and stored at −80°C until further analysis.

2.7.3. Analysis of AChE activity and ACh content levels in brain tissues

Some portions of the cerebral cortices and hippocampi were homogenised in 20 mM PBS (pH 7.6, 1:10 w/v) on ice, and the homogenates were centrifuged at 12000 × *g* for 15 min at 4°C. The supernatants were used to measure the activity of AChE through a validated UPLC-MS/MS method (Liu et al., 2014). Briefly, a mixture of 30 µL of ACh (200 µM) and 30 µL of supernatant was added in a 1.5 mL Eppendorf tube, and the reaction was terminated after co-incubation for 5 min and 10 min at 25°C by the addition of 180 µL of cold acetonitrile (0°C), respectively. Each sample was prepared in triplicate. After being centrifuged at 12000 × *g* for 10 min, the Ch content in the supernatant of the reaction mixture was measured by UPLC-MS/MS (Liu et al., 2014). The activity of AChE was calculated using the following equation:

The activity of AChE ($unit \cdot g^{-1}$) = K × (Mean $C_{10\ min}$–Mean $C_{5\ min}$)/ΔT.

where K represents the dilution factor of the sample, Mean $C_{10\ min}$ represents the mean content of Ch in triplicate samples co-incubated for 10 min, Mean $C_{5\ min}$ represents the mean content of Ch in triplicate samples co-incubated for 5 min and ΔT represents the time difference to terminate reaction.

The remaining supernatants of the cerebral cortices and hippocampi were detected by the validated UPLC-MS/MS method (Liu et al., 2014) for the determination of the ACh and Ch contents.

2.7.4. Analysis of choline acetyltransferase activity in brain tissues

The levels of ChAT in the cerebral cortex and hippocampus homogenates were measured with commercially available assay kits in accordance with the manufacturer's protocols. The levels of ChAT in the cerebral cortex and hippocampus tissues were normalizedand expressed as unit·g^{-1} tissue.

2.7.5. Western blot analysis

The hippocampus and cortex sections of mice were homogenised on ice with CellLytic^{TM}MT mammalian tissue lysis reagent (Sigma, C3228), which contains protease and phosphatase inhibitor cocktails (Sigma, P3840). The supernatant was separated from the homogenate, which was centrifuged at 12000 ×*g* for 10 min at 4°C. Protein concentration was quantified by BCA assay. Thereafter, 20 μg of protein from each sample was electrophoresed by 10% SDS-PAGE and transferred to PVDF membrane (Millipore, Temecula, CA, USA). The membrane was incubated with blocking solution (5% BSA) for 1 h at room temperature and then incubated overnight with primary antibodies against AChE (Millipore, Temecula, CA, USA), ChAT and GAPDH (Abcam, Cambridge, UK) at 4°C. The membrane was then washed five times with PBS containing 0.1% Tween 20 (PBST), incubated with horse radish peroxidase-conjugated secondary antibodies for 1 h at room temperature, washed five times with PBST and visualised with ECL prime kit (GE Healthcare, NA, UK; He et al., 2015).

2.8. Acute toxicity test for d-VAS and l-VAS in mice

In the acute toxicity study, Kunming mice were divided into 12 groups (five males and five females for each group) after an appropriate pre-experiment. The mice underwent fasting for 12 h with water *ad libitum* before treatment. *l*-VAS was orally administered at doses of 219, 258, 303, 357, 420 and 494 mg·kg^{-1}, and *d*-VAS was orally administered at doses of 186, 219, 258, 303, 357 and 420 mg·kg^{-1}, respectively. The general behaviours of the mice were observed continuously for 1 h after the treatment, intermittently for 4 h and then over 24 h. The mice were further observed for up to 14 days after

treatment to search for any sign of toxicity and death. The median lethal dose (LD_{50}) values and 95% confidence limits of *d*-VAS and *l*-VAS were calculated by Bliss method.

2.9. Isolation and purification of d-VAS and l-VAS

The VAS enantiomers were separated by using a CHIRALPAK AY-H column (0.46 cm × 15 cm, Daicel Chemical Industries, Ltd., Tokyo, Japan) with a flow-rate of 0.5 $mL \cdot min^{-1}$ and UV detection at 210 nm with ethanol/diethanol amine ration of 100/0.1 (v/v). The HPLC chromatogram was shown in Supplementary Fig. S2. Fraction solutions of 6.129 min and 9.297 min were collected and concentrated *in vacuo* to yield residues. The purities of *d*-VAS and *l*-VAS were determined to be more than 98% through the normalization of the peak areas detected by HPLC-DAD (Fig. S2B and S2C). The fraction solution of 6.129 min was confirmed as *l*-VAS by the specific rotation value of −43.67 (c=0.1 $mg \cdot mL^{-1}$, ethanol) after setting the temperature at 20°C. The relatively specific rotation value of the fraction solution of 9.297 min was +41.83 (c=0.1 $mg \cdot mL^{-1}$, ethanol), which was confirmed as *d*-VAS.

2.10. Isolation and purification of glucuronide metabolites d-VASG and l-VASG

Rac-VAS was administered to guinea pigs (n=10) by *gavage* in a dose of 100 $mg \cdot kg^{-1}$, and approximately 0.44 L of urine samples from the guinea pigs were subjected to MCI Gel CHP 20P column chromatography (4.5 × 60 cm; 1000 mL). The column was then eluted with a gradient system of methanol–water (0:100; 5:95; 10:90; 20:80; 30:70; 50:50; 100:0). The elution profiles of the metabolites were obtained from 10% and 20% methanol fractions. Both fractions were concentrated *in vacuo* to yield residues, which were then dissolved in a small amount of water and purified by semi-preparative HPLC.

Semi-preparative HPLC was performed with a ZORBAX SB-C18 column (9.4 mm × 25 cm, 5 μm; Agilent, USA) at 30°C in an LC3000 liquid chromatograph (Beijing Tong Heng Innovation Technology Co., Beijing, China). The detection wavelength was set at 280 nm. The mobile phase consisted of methanol (A) and 0.1% aqueous formic acid (B). The mixture of VASG enantiomers (138 mg) was obtained using a gradient elution of 0 min to 10 min (5% to 20% A, with) at a flow rate of 3 $mL \cdot min^{-1}$. The purity of the mixture of VASG enantiomers detected through HPLC-DAD and UPLC-MS/MS was more than 98% after area normalization. The separation and preparation of *d*-VASG and *l*-VASG were carried out on a Spursil C18 column (9.4 mm × 25 cm, 5μm; Dikma Limited, CA, USA). Finally, pure *d*-VASG and *l*-VASG were prepared.

2.11. Statistical analysis

All data were analysed on SPSS 18.0 and expressed as mean ± standard deviation (SD) unless otherwise indicated. The escape latency and escape rate data in MWM test were analysed using two-way analysis of variance (ANOVA) with repeated measures. The other behavioural data and the biomarker changes *in vivo* and *in vitro* were analysed by one-way ANOVA followed by Tukey's Post Hoc Test. The pharmacokinetic parameters were also expressed as the mean ± standard deviation. The plasma concentration versus time curves were plotted and all the pharmacokinetic data were processed using the noncompartmental pharmacokinetics data analysis software program PK solutions 2™ (Summit Research Services, USA). The following pharmacokinetic parameters of quantitative compounds were calculated: absorption rate constant (k_a), absorption half-life ($t_{1/2ka}$), distribution rate constant (k_d), distribution half-life ($t_{1/2kd}$), elimination rate constant (k_e), elimination half-life ($t_{1/2ke}$), apparent volume of distribution (V_d/F), apparent clearance rate (CL/F), and mean residence time (MRT). The maximum peak concentration (C_{max}), the time of maximum plasma concentration (T_{max}) and area under the plasma concentration versus time curve from zero to time t ($AUC_{(0-t)}$) were obtained directly from the observed concentration versus time data. The area under the plasma concentration versus time curve from zero to infinity ($AUC_{(0-\infty)}$) was calculated by means of the trapezoidal rule with extrapolation to infinity with a terminal k_e. For all statistical tests, the value of $p < 0.05$ was regarded as significant.

3. Results

3.1. Metabolic diversity of VAS enantiomers in vitro

3.1.1. Elimination rates of rac-VAS, d-VAS and l-VAS in HLM

The elimination rates of *rac*-VAS, *d*-VAS and *l*-VAS were determined in HLM *in vitro*. The results were shown in Supplementary Fig. S3. After incubation of 2 h, the residues of *rac*-VAS, *d*-VAS, and *l*-VAS were 68.2 ± 8.0%, 72.4 ± 10.4%, and 44.7 ± 10.5%, with $t_{1/2}$ of 227.5±3.8, 294.1±28.2, and 131.4 ± 18.3 min, and the CL_{int} of 61.2±1.3, 48.4 ± 6.2, and 118.2 ± 14.3 $\mu L \cdot min^{-1} \cdot mg^{-1}$ protein, respectively, indicating that the elimination rate of *l*-VAS was significantly faster than those of *d*-VAS ($p < 0.01$).

3.1.2. Formation rates of metabolites in pooled HLM and pre-clinical liver microsomes

The glucuronidation metabolites *d*-VASG and *l*-VASG were detected in the HLM after incubation with 500 μM *rac*-VAS, *l*-VAS and *d*-VAS (Supplementary Fig. S4). The rate of the *d*-VASG production (peak area, 37933.5 ± 2814.99) was significantly lower than that of *l*-VASG (peak area, 201368.5 ± 4331.03) in HLM after incubation with rac-VAS. The amount of *d*-VASG production (peak area, 6824 ± 354.97) accounted for 3.21% of the amount of *l*-VASG production (peak area: 212721.5 ± 9594.73) in HLM after incubation with the *l*-VAS (Fig. S4B). However, the area responses of *d*-VASG and *l*-VASG were 27404 ± 1890.80 and 3906.5 ± 228.40, respectively, when the substrate was *d*-VAS (Fig. S4C). Although both *l*-VASG and *d*-VASG could be detected in the *d*-VAS group, but the *l*-VASG production only accounted 14.2% of *d*-VASG. These data implied that *l*-VAS was prone to be metabolized into *l*-VASG, and *d*-VAS was metabolized into *d*-VASG, but the rate of *l*-VASG production was significantly faster than that of *d*-VASG in HLMs with the same substrate concentration ($p < 0.01$). These results indicated that stereoselective metabolism occurred between *d*-VAS and *l*-VAS, and *l*-VAS was more prone to be metabolized by glucuronidation in HLM.

The glucuronidation metabolites *d*-VASG and *l*-VASG were evaluated in the pre-clinical liver microsomes after incubation with 500 μM *rac*-VAS, *l*-VAS and *d*-VAS (Supplementary Fig. S5). The rates of the *d*-VASG and *l*-VASG production in some pre-clinical liver microsomes (MoLM, BLM, SLM, DLM, GLM, RLM, MLM, PLM, and RaLM) were significantly faster than in HLM after incubation with 500 μM *rac*-VAS, *l*-VAS or *d*-VAS. It is worth noting that the rates of the *d*-VASG and *l*-VASG production in GLM was the fastest among other pre-clinical liver microsomes, and the production *d*-VASG and *l*-VASG in GLM were also comparable after incubation with *rac*-VAS. The urinary excretion of *d*-VASG and *l*-VASG in guinea pigs were also comparable after performing oral administration of *rac*-VAS on rats (data was not shown). It benefited from the result that the standard substances of *d*-VASG and *l*-VASG were isolated and obtained from urine of guinea pigs after oral administration of *rac*-VAS. In additional, it was found that the rate of the *l*-VASG production was faster than *d*-VASG in various pre-clinical liver microsomes, except for GLM. All of these results indicated that the glucuronidation metabolism of VAS or its enantiomers has certain difference in species.

3.1.3. Effect of UGT inhibitors on production rates in pooled HLM

The inhibitory reaction activities for the VASG enantiomer formation caused by niflumic acid (UGT1A9 inhibitor) and diclofenac (UGT2B15 inhibitor) were below 35% in the *rac*-VAS and VAS

enantiomers, as shown in Fig. 1, no matter the substrate was *rac*-VAS or VAS enantiomers. These results indicated that UGT1A9 and UGT2B15 were the major enzymes responsible for the glucuronidations of *l*-VAS and *d*-VAS.

3.1.4. Identification of UGT isoforms in recombinant human UGT systems

The results of recombinant human UGTs (rhUGTs) assay and specific inhibitory studies were displayed in Fig. 2. They showed that rhUGT1A1, rhUGT1A3, rhUGT1A7, rhUGT1A8, rhUGT1A9, rhUGT2B4, rhUGT2B7, rhUGT2B15 and rhUGT2B17 were involved in the metabolism of *rac*-VAS and *l*-VAS to *l*-VASG, and the most active among them were rhUGT1A9 and rhUGT2B15 (Fig. 2A and 2B). rhUGT1A1, rhUGT1A3, rhUGT1A9, rhUGT2B4 and rhUGT2B7 involved in catalysing the metabolism of *d*-VAS to *d*-VASG, and rhUGT1A9 was the most active (Fig. 2C). Different metabolic enzymes could possibly induce stereoselective metabolic differences between *d*-VAS and *l*-VAS.

3.1.5 Enzyme kinetics studies on the formation of glucuronidation metabolites in HLM and rhUGT isoenzymes

The best fit of data shown in Fig. 3 and Fig. 4 was obtained using the double Michaelis-Menten equation for enzyme kinetics. The Eadie-Hofstee transformations revealed evidence of enzyme kinetics in HLM, as well as in rhUGT1A9 and rhUGT2B15. The V_{max} of the metabolic conversion of *d*-VAS to *d*-VASG (0.35 ± 0.09 pmol·min^{-1}·mg^{-1} protein) was much lower than that of *l*-VAS to *l*-VASG (8.77 ± 0.72 pmol·min^{-1}·mg^{-1} protein) in HLM (Table S2). Similarly, the V_{max} of metabolic conversion of *d*-VAS to *d*-VASG (0.84 ± 0.08 pmol·min^{-1}·mg^{-1} protein) was much lower than that of *l*-VAS to *l*-VASG (1.72 ± 0.52 pmol·min^{-1}·mg^{-1} protein) in rhUGT1A9 (shown in Table 1; $p < 0.05$). Moreover, the *CL* of the metabolism of *l*-VAS to *l*-VASG (0.015 ± 0.001 L·min^{-1}·mg^{-1} protein, $p < 0.001$) was significantly higher than that of *d*-VAS (0.003 ± 0.001 L·min^{-1}·mg^{-1}protein, $p < 0.001$) in HLM. These data illustrated that *l*-VAS is tend to be metabolized into *l*-VASG. Furthermore, *d*-VASG formation was inadequate to calculate the kinetic parameters in rhUGT2B15.

*3.2. In vivo stereoselective pharmacokinetic of d-*VAS and *l*-VAS *in rats*

The plasma concentration time curves of *d*-VAS and *l*-VAS in rats after intravenously and orally administration of *d*-VAS and *l*-VAS were shown in Fig. 5. The similar profiles were obtained for both *d*-VAS and *l*-VAS after intravenously and orally administration. To compare the difference of

pharmacokinetics between *d*-VAS and *l*-VAS and their main metabolites in the plasma of rats, the pharmacokinetics parameters after intravenously and orally administration of *d*-VAS and *l*-VAS were calculated and summarized in Table 2 and Table 3, respectively. It could be seen from Fig. 5A and 5B, similar profiles were obtained for both *d*-VAS and *l*-VAS after intravenously and orally administration. T_{max} could be used to define the time of maximum plasma concentration after orally administration, which is similar for *d*-VAS and *l*-VAS. However, differences observed in C_{max} and *AUC* values between *d*-VAS and *l*-VAS after intravenously and orally administration. The $AUC_{(0-\infty)}$ and C_{max} after the intravenously administration of *d*-VAS were nearly 1.4-fold and 1.2-fold higher than that of *l*-VAS, respectively (Table 2). The $AUC_{(0-\infty)}$ and C_{max} after the oral administration of *d*-VAS were nearly 1.6-fold and 1.7-fold higher than that of *l*-VAS, respectively (Table 3).

The absolute bioavailability (*F*) of *d*-VAS and *l*-VAS were 80.6% and 65.7%, respectively, implying that the first pass effect of *d*-VAS was lower than that of *l*-VAS. Furthermore, the $t_{1/2Ke}$ and *MRT* after the intravenously administration of *d*-VAS were nearly 2.6-fold and 2.2-fold longer than that of *l*-VAS, the $t_{1/2Ke}$ after the orally administration of *d*-VAS was nearly 1.3-fold longer than that of *l*-VAS, and *d*-VAS had significantly slower elimination rates in plasma after oral administration ($p < 0.05$; Table 2) and intravenous administration ($p < 0.001$; Table 3). After intravenously and orally administration of *l*-VAS, the plasma exposure ($AUC_{(0-\infty)}$) of *l*-VASG was more 5.2-fold and 46.3-fold higher than that of *d*-VASG (Fig. 5C and 5D). Similarly, the *l*-VASG and *d*-VASG enantiomers were both detected in the plasma when *d*-VAS was intravenously and orally administered (Fig. 5E and 5F), but the plasma exposure of *l*-VASG was also 1.2-fold and 1.2-fold higher than that of *d*-VASG (Tables 2 and 3).

3.3. Inhibitory activity of d-VAS and l-VAS on AChE and BChE in vitro

The IC_{50} values of the technical mixtures of two stereoisomers with different proportions of AChE and BChE were compared. As indicated in Fig. 6, both *d*-VAS and *l*-VAS showed potent inhibitory activities against AChE and BChE, but no significant difference was observed between *d*-VAS (IC_{50}: 1.73 ± 0.21 μM) and *l*-VAS (IC_{50}: 1.49 ± 0.03 μM) when the values were plotted against AChE (Fig. 6). On the contrary, significant differences between the IC_{50} values of *d*-VAS and *l*-VAS when the values were plotted against BChE. The IC_{50} values decreased as *l*-VAS/*d*-VAS ratio decreased. With respect to the inhibition of BChE inhibitory activity, the IC_{50} value of *d*-VAS (0.03 ± 0.00 μM) was 30 times higher than that of *l*-VAS with IC_{50} of 0.98 ± 0.19 μM (Fig. 6).

3.4. Molecular docking of d-VAS and l-VAS with human AChE and BChE

The molecular binding abilities of *d*-VAS and *l*-VAS with hAChE and hBChE were illustrated in Fig. 7. The binding pocket and ligand binding of *d*-VAS were similar with that of *l*-VAS when hAChE and hBChE were used for the structural composite. Both *d*-VAS and *l*-VAS could bind to the catalytic active site (CAS) and subsequently inhibit the activities of compounds (Changeux, 1996; Rosenberry et al., 2008). In our study, *d*-VAS and *l*-VAS ranked first and thus were selected for subsequent analyses. AChE molecular docking results revealed that a hydrogen bond could be generated between Trp439 and one hydrogen atom in the benzene ring in *d*-VAS. A strong π-π hydrophobic interactions could be observed (Fig. 7A and 7B), and a hydrogen atom in the hydroxyl group of *l*-VAS formed a hydrogen bond with H_2O (Fig. 7C and 7D). In the BChE molecular dock, a weak hydrogen–benzene interaction was formed by the hydrogen on the C_{11} of *d*-VAS. The other hydrogen atom on the same position formed a hydrogen bond with Glu197. An oxygen atom in the hydroxyl group formed a hydrogen bond with Gly116, and the pyridine ring of *d*-VAS was characterized by a strong π–π hydrophobic interaction between Trp82 and the benzene ring of *d*-VAS (Fig. 7E and 7F). The π–π hydrophobic interaction and hydrogen bond of *l*-VAS with Glu197 were the same as those observed in *d*-VAS. However, a hydrogen bond between hydrogen on C_{11} and His438 was present, and the hydrogen–benzene interaction was absent in *l*-VAS (Fig. 7G and 7H).

In summary, the ability of VAS enantiomers to combine with AChE was slightly weaker than that with BChE because of the weaker affinity of *d*- and *l*-VAS with AChE (the score of GBI/WAS dG: –6.902 and –6.898) compared with BChE and the stronger combing ability of *d*-VAS to combine with hBChE (the score of GBI/WAS dG: -7.398) compared with *l*-VAS (the score of GBI/WAS dG: -7.135). These results were in agreement with the *in vitro* AChE and BChE inhibition assay described above, where inhibitory activity of *d*-VAS against BChE was stronger than that against *l*-VAS.

3.5. VAS enantiomers attenuated cognitive impairments induced by scopolamine in mice

To explore whether *rac*-VAS, *d*-VAS and *l*-VAS prevent acute memory impairment, we measured their anti-amnesic effects in scopolamine-induced and memory-deficient mice by the MWM tasks. In the hidden platform–swimming trials, the scopolamine-treated mice showed markedly impaired memory in their path length on the third, fourth and fifth testing days, respectively (Fig. 8A, 11.71 ± 5.56 m *vs*. 5.80 ± 2.09 m, $p < 0.01$; 14.99 ± 9.06 m *vs.* 4.98 ± 3.56 m, $p < 0.05$ and 15.67 ± 5.04 m *vs.*

3.37 ± 1.99 m, $p < 0.001$), and the escape latency on the fourth and fifth testing days, respectively (Fig. 8B, 39.25 ± 20.12 s *vs.* 25.13 ± 16.50 s, $p < 0.01$; 47.00 ± 15.20 s *vs.* 21.43 ± 17.73 s, $p < 0.05$). By contrast, both *rac*-VAS and *d*-VAS could effectively shorten the path length on the third testing day (6.76 ± 4.48 m *vs.* 11.71 ± 5.56 m, $p < 0.05$; 6.62 ± 2.48 m *vs.* 11.71 ± 5.56 m, $P < 0.05$), as well as with the *l*-VAS and donepezil (8.40 ± 2.78 m *vs*. 14.99 ± 9.06 m, $p < 0.05$; 8.45 ± 4.85 m *vs.* 14.99 ± 9.06 m, $p < 0.05$) on the fourth testing day (Fig. 8A). Moreover, on the fourth testing day, *rac*-VAS, *d*-VAS, *l*-VAS and donepezil could effectively shorten the escape latency of scopolamine-treated mice (25.37 ± 22.99 s *vs.* 39.25 ± 20.12 s, $p < 0.05$; 23.00 ± 9.90 s *vs.* 39.25 ± 20.12 s, $p < 0.05$; 26.43 ± 11.82 s *vs.* 39.25 ± 20.12 s, $p < 0.05$ and 22.71 ± 10.84 s *vs.* 39.25 ± 20.12 s, $p < 0.05$; Fig. 8B).

One day after the last hidden platform-swimming test, the spatial probe test was performed to determine whether mice could memorise the location of the platform. The spatial memory of scopolamine-induced mice was significantly damaged in contrast to those in the control group. The mice passed less through the target zone where the hidden platform was placed 24 h before (Fig. 8C and 8D, $p < 0.001$). Conversely, mice treated with *rac*-VAS, *d*-VAS and *l*-VAS at 15 $mg \cdot kg^{-1}$ and donepezil at 3 $mg \cdot kg^{-1}$ crossed the site more often than those by treated with scopolamine alone ($p < 0.05$).

3.6. d-VAS increased ACh content by moderating the activities of AChE and ChAT

The ACh and Ch contents detected by UPLC MS/MS in the cerebral cortices were shown in Fig. 9A and 9B. The ACh contents in the scopolamine-treated mice were significantly lower ($p < 0.05$) than those in the control. By contrast to the scopolamine-treated mice, the ACh contents in mice treated with *d*-VAS showed significant increase ($p < 0.05$), and became higher than those in mice treated with *l*-VAS. No difference was observed on the Ch contents among the treatment group, scopolamine group, and donepezil group, by comparing to that in control group.

In order to explore how VAS enantiomers affecting on ACh content *in vivo*, the activities of AChE in the cerebral cortex and hippocampus, and the activities of ChAT in the cerebral cortex of scopolamine-induced mice were measured. Long-term *d*-VAS and *l*-VAS treatment for 15 days could significantly inhibit AChE activity (Fig. 9C and Fig. 9D) and decrease the protein expression of AChE in the cerebral cortex and hippocampus (Fig. 9F, Fig. 9G, Fig. 9I, and Fig. 9J), especially for *d*-VAS ($p < 0.01$ and $p < 0.05$, respectively). On the contrary, the activity of ChAT was enhanced in the cerebral

cortex (Fig. 9E) and ChAT protein expression was increased in the cerebral cortex and hippocampus after treatment with rac-VAS, *d*-VAS and *l*-VAS. But, treatments with *d*-VAS and *l*-VAS did not produce significant difference on the activity and expression of ChAT (Fig. 9F, Fig. 9H, Fig. 9I, and Fig. 9K).

3.7. Acute toxicity of d-VAS and l-VAS in mice

The results of acute toxicity tests of *d*-VAS and *l*-VAS in mice were shown in Supplementary Table S3. The LD_{50} values of *d*-VAS and *l*-VAS after oral administration into mice were 282.51 $mg \cdot kg^{-1}$ (95% confidence limits 250.23 - 315.76 $mg \cdot kg^{-1}$) and 319.75 $mg \cdot kg^{-1}$ (95% confidence limits 271.85 - 363.39 $mg \cdot kg^{-1}$) by Bliss method, respectively. These finding indicated a slight lower LD_{50} value of *d*-VAS than *l*-VAS in mice, but there were no significant differences.

4. Discussion

On chiral drugs, the FDA has regulated the study of the pharmacokinetics, pharmacodynamics and toxicology properties of pure isomers (FDA, 1992). For example, clausenamide (Clau) is an active compound originally extracted from the traditional Chinese herbal medicine, *Clausena lansium*, which has four chiral centres. The Clau eutomer (-)-Clau and the distomer (+) has been demonstrated to improve cognitive function in normal physiology and pathological conditions (Chu et al., 2016). In addition, bambuterol is a long-acting β adrenoceptor agonist and cholinesterase inhibitor used in the treatment of asthma, it is administered as a racemic mixture, and the recent study has found R-bambuterol showing a stronger inhibitory effect than S-bambuterol in BChE stereoselective inhibition (Pistolozzi et al., 2015). Similarly, the present study focused on the stereoselectivity of VAS enantiomers on improvement of learning and memory abilities, and aimed to find out which of *d*-VAS and *l*-VAS is the dominant enantiomer.

AD is a common neurodegenerative disease, and AChE and BChE are the two enzymes involved in breaking down the neurotransmitter ACh. Many researchers consider ChE inhibitors, such as physostigmine and galantamine, to be selective for AChE (Mukherje et al., 2007). These inhibitors could prolong the availability of acetylcholine. Some studies revealed that AChE predominates in the healthy brain, with BChE considered to play a minor role in regulating brain ACh levels. However, BChE activity progressively increases in patients with AD, while AChE activity remains unchanged or declines (Lam et al., 2009; Greig et al., 2002; 2005). Thus, AD treatment has been focused on BChE

inhibition rather than on AChE in recent years (Giacobini, 2004; Greig et al., 2002), and BChE has become as a new therapeutic target and diagnostic marker in AD treatment. Huperzine A, a quinolizidine alkaloid from *Huperzia serrata*, was found to reversibly inhibit AChE (IC_{50}=47 nM) and BChE (IC_{50}=30 nM) (Giacobini, 2004), showing potential use in the treatment of AD at an advance stage. The *in vitro* anticholinesterase activity assays of VAS enatiomers indicated that *d*-VAS has a stronger inhibitory activity against BChE than *l*-VAS. The inhibitory activity of *d*-VAS against BChE (IC_{50}= 0.029 ± 0.001 μM) was similar to that of huperzine A.

As anti-cholinergic drug, scopolamine impairs cholinergic system activity by acting on muscarinic receptor and increase AChE activity. Therefore, the scopolamine-induced memory deficits model has been widely used in screening for candidate drugs with cognitive improvement (Gutierres et al., 2014; Liu et al., 2017). As a common cholinesterase inhibitor, donepezil has been used to improve cognition and behavior of AD patients in clinic. In the present study anti-amnesic effects were measured in scopolamine-induced and memory-deficient mice through MWM tasks to determine whether *rac*-VAS, *d*-VAS and *l*-VAS prevent acute memory impairment. The results indicated that *rac*-VAS, *d*-VAS and *l*-VAS administration could significantly improve spatial learning and memory in cognitively impaired mice. The ACh content in the mouse cortices after *d*-VAS oral administration increased, and the activity of ChE in the mouse cortices and hippocampi after *d*-VAS oral administration decreased. However, the behavioral test disclosed few differences between VAS enantiomers and *rac*-VAS. The reason may be multifaceted. Dysfunction of cholinergic system, neuroinflammation, oxidative stress and amyloid plaque deposition were the early events in the development and progression of AD (Hamodat et al., 2017; Kanamaru et al., 2015; Dong et al., 2004). Intraperitoneal injection of scopolamine not only could cause memory impairment and cholinergic system dysfunction but also could trigger ROS and inflammation production in the brain (Tao et al., 2014; Xian et al., 2015; Guo et al., 2016). Thus, *d*-VAS and *l*-VAS not only could improve the learning and memory of cognitively impaired mice by regulating cholinergic nervous system but also acting on other routes.

The metabolism of *rac*-VAS was systematically investigated *in vitro* and *in vivo* in our previous study, and the glucuronidation of VAS was one of the most important metabolic pathways (Liu et al., 2015b; Liu et al., 2015c). In the present study, the stereoselective glucuronidation metabolism of VAS enantiomers was investigated. In order to obtain quantitative experimental results, the reference

standard substances of *d*-VASG and *l*-VASG were isolated and purified. The *in vitro* phase II glucuronidation metabolite of *rac*-VAS was incubated in the liver microsomes of 11 mammalian species (human, monkey, camel, bull, sheep, dog, guinea pig, rat, mouse, pig and rabbit; Supplementary Fig. S5A). The production rates of *d*-VASG and *l*-VASG significantly vary among different mammalian liver microsomes, and the highest production rates were observed in guinea pigs liver microsomes, implying that guinea pigs were the most suitable species for preparing the *d*-VASG and *l*-VASG metabolites. The urinary excretion of *d*-VASG and *l*-VASG in guinea pigs were also comparable after performing oral administration of *rac*-VAS on rats (data was not shown). Thus, the *d*-VASG and *l*-VASG from the urine of guinea pigs were isolated and purified after performing oral administration of 100 $mg \cdot kg^{-1}$ of *rac*-VAS. When the substrate was *d*-VAS or *l*-VAS, the diversity of glucuronidation metabolite in 11 mammalian liver microsomes was prominent (Fig. S5B and S5C). Given the significant differences among the production rates of *d*-VASG and *l*-VASG was observed in different liver microsomes, it could provide an available animal models to prepare the desired metabolites, and it could provide a very useful strategy for the study of other similar drugs.

The glucuronidation metabolism of *rac*-VAS, *d*-VAS and *l*-VAS were detected in the HLM (Supplementary Fig. S5). The amount of *d*-VASG and *l*-VASG production showed a significant difference in the *rac*-VAS group. The amount of *l*-VASG was significantly higher than that of *d*-VASG, indicating that the rate of *l*-VASG production was significantly faster than that of *d*-VASG in HLM. Subsequent studies on *d*-VAS and *l*-VAS in HLM have further confirmed this conclusion. *l*-VAS could be metabolized into *l*-VASG and *d*-VASG, and *d*-VAS could also be metabolized into *l*-VASG and *d*-VASG in HLM (Supplementary Fig. S4). Similar results have been found in the pharmacokinetic study of VAS enantiomers in rats (Table 2 and Table 3). However, on the UGT isoforms assay, *d*-VAS and *l*-VAS could be only metabolized into *d*-VASG and *l*-VASG, respectively (Fig. 2). The complex and variable metabolic enzymes, a large number of enterobacteria and a variety of endogenous substances in liver microsomes and mice, may be the reasons for the conversion configuration of *l*-VASG and *d*-VASG (Zhang et al., 1994; Reist et al., 1998; Ma et al., 2005). However, the conversion configuration between *l*-VAS and *d*-VAS has not been found in HLM *in vitro* (Supplementary Fig. S6), and in rats plasma by a pilot test *in vivo* (Supplementary Fig. S7).

In addition, the results of rhUGTs assay indicated that both UGT1A9 and UGT2B15 participated in catalysing *l*-VAS to *l*-VASG (Fig. 2B), and only UGT1A9 was the main enzymes involved in metabolism of *d*-VAS to *d*-VASG. Enzyme kinetics studies indicated that the V_m of rhUGT1A9 and rhUGT2B15 for metabolizing *l*-VAS to *l*-VASG were 1.72 ± 0.52 pmol·min^{-1}·mg^{-1} protein and 2.01 ± 0.00 pmol·min^{-1}·mg^{-1} protein, respectively. And the V_m of rhUGT1A9 for the metabolic conversion of *d*-VAS to *d*-VASG was 0.84 ± 0.08 pmol·min^{-1}·mg^{-1} protein. It indicated that not only different rhUGT isoforms could metabolize VAS enantiomers but the metabolic capacity of a given UGT isoform could induce the stereoselective metabolic differences between *d*-VAS and *l*-VAS.

The results of *in vivo* pharmacokinetics study disclosed that the plasma exposure of *d*-VAS was 1.3-fold and 1.6-fold higher than that of *l*-VAS and the major glucuronidation metabolite *d*-VASG was approximately one-tenth of *l*-VASG in rats after intravenous and oral administration of *d*-VAS and *l*-VAS, respectively. In lights of the exposure difference, the different metabolic enzymes responsible for VAS enantiomers, such as UGT1A9 and UGT2B15, might play a key role in pharmacokinetics processes of *d*-VAS and *l*-VAS.

In a previous *in vitro* study, the AChE and BChE inhibitory activities of VAS and its major metabolites were investigated, the results indicated that most metabolites maintain potential inhibitory activity against AChE and BChE but is weaker than that of the prototype VAS, implying that VAS undergoes metabolic inactivation process *in vivo* with respect to cholinesterase inhibitory activity (Liu et al., 2015b; Liu et al., 2015c). In the present study, the plasma exposure level of *d*-VAS was higher than in *l*-VAS after intravenous or oral administration of the same dose of *d*-VAS or *l*-VAS in rats. In addition, *d*-VAS displayed a stronger BChE *in vitro* inhibitory activity than that of *l*-VAS at same concentration. The activity of AChE in the mouse cortex and hippocampus was extensively decreased more after oral administration of *d*-VAS than that of *l*-VAS, implying that excessive cholinesterase inhibition was more likely to occur in high doses of *d*-VAS in acute toxicity test.

The evaluation of the stereoselective toxicity of different enantiomers is extremely important. Despite all this, published studies on the toxicity of VAS to mammals were rare. It was reported that the LD_{50} values after oral administration of VAS in mice and rats were 290 and 640 mg·kg^{-1} (Claeson et al., 2000). In the present study, the LD_{50} values of *d*-VAS and *l*-VAS after oral administration in mice were 282.51 mg·kg^{-1} (95% confidence limits 250.23 - 315.76 mg·kg^{-1}) and 319.75 mg·kg^{-1} (95% confidence

limits 271.85 - 363.39 $mg \cdot kg^{-1}$) by the Bliss method, respectively. Thus, *d*-VAS and *l*-VAS could experience the same acute toxicity with similar LD_{50} values.

Species difference exists in physiology, anatomy, and metabolic enzymes expression/activity (Fujiwara, et al., 2018) among different species of animals and human. There are great pressures for extrapolating data obtained from animals to clinical trial and toxicity of new drugs candidate.

In conclusion, it was firstly confirmed that VAS enantiomers exhibit significantly stereoselective anti-amnesic effects, metabolic, and pharmacokinetic properties *in vitro* and *in vivo*. Based on these proofs, it could be believed that *d*-VAS might be a dominant configuration suitable as a drug candidate for AD treatment. Of course, there is still much more challenging researches to be done in the future, such as clinic pharmacokinetics, pharmacodynamics, and safety evaluation, etc.

Conflict of interest

The authors declare no conflict of interest.

Acknowledgments

This work was supported by the National Natural Science Foundation of China and Xinjiang Uygur Autonomous Region of China (No. U1130303), the National Nature Science Foundation of China (No. 81173119), the Key Project of Ministry of Science and Technology of China (2012ZX09103201-051) awarded to Professor Changhong Wang for financial support of this study. Yudan Zhu and Wei Liu were contributed equally to this work.

Reference

Ali, S.K., Hamed, A.R., Soltan, M.M., El-Halawany, A., Hegazy, U. and Hussein, A., 2016. Kinetics and molecular docking of vasicine from Adhatodavasica: An acetylcholinesterase inhibitor for Alzheimer's disease. *S. Afr. J. Bot*. **104,** 118-124.

Atal, C.K., 1980. Chemistry and pharmacology of vasicine: A new oxytocic and abortifacient. *Jammu: Regional Res. Lab*.

Ballard, T.E., Wang, S., Cox, L.M., 2016. Application of a micropatterned co-cultured (MPCC) hepatocyte system to predict preclinical and human specific drug metabolism. *Drug Metab. Dispos.* **44,** 172-179.

Bartl, J., Palazzesi, F., Parrinello, M., Leif, H., Riederer, P., Walitza, S., Grünblatt, E., 2017. The impact of methylphenidate and its enantiomers on dopamine synthesis and metabolism *in vitro*. *Prog. Neuro-Psychoph*. **79,** 281-288.

Changeux, J.P., 1966. Responses of acetylcholinesterase from Torpedo marmorata to salts and curarizing drugs. *Mol. Pharmacol*. **2,** 369-392.

Chu, S., Liu, S., Duan, W., Cheng, Y., Jiang, X., Zhu, C. and Yu, X., 2016. The anti-dementia drug candidate, (−)-clausenamide, improves memory impairment through its multi-target effect. *Pharmacol. Ther*. **162,** 179-187.

Claeson, U.P., Malmfors, T., Wikman, G., Bruhn, J.G., 2000. Adhatoda vasica: a critical review of ethnopharmacological and toxicological data. *J. Ethnopharmacol*. **72,** 1-20.

Dong, H., Goico, B., Martin, M., Csernansky, C.A., Bertchume, A. and Csernansky, J.G., 2004. Modulation of hippocampal cell proliferation, memory, and amyloid plaquedeposition in APPsw (tg 2576) mutant mice by isolation stress. *Neuroscience* **127,** 601-609.

FDA, Policy statement for the development of new stereoisomeric drugs. 1997. http://www.fda.gov/Drugs/Guidance Compliance Regulatory Information/Guidances /ucm122883htm.

Fujiwara, R., Yoda, E., Tukey, R.H., 2018. Species differences in drug glucuronidation: Humanized UDP-glucuronosyltransferase 1 mice and their application for predicting drug glucuronidation and drug-induced toxicity in humans. *Drug Metab. Pharmacok*. **33**, 9-16

Giacobini, E., 2004. Cholinesterase inhibitors: new roles and therapeutic alternatives, *Pharmacol. Res.* **50,** 433-440.

Greig, N.H., Lahiri, D.K., Sambamurti, K., 2002. Butyrylcholinesterase: an important new target in Alzheimer's disease therapy. *Int. Psychogeriatr.* **14,** 77-91.

Greig, N.H., Utsuki, T., Ingram, D.K., Wang, Y., Pepeu, G., Scali, C., Chen, D., 2005. Selective butyrylcholinesterase inhibition elevates brain acetylcholine, augments learning and lowers Alzheimer -amyloid peptide in rodent. *Proc. Natl. Acad. Sci. USA* **102,** 17213-17218.

Guo, C., Shen, J., Meng, Z., Yang, X. and Li, F., 2016. Neuroprotective effects of polygalacic acid on scopolamine-induced memory deficits in mice. *Phytomedicine* **23,** 149-155.

Gutierres, J.M., Carvalho, F.B., Schetinger, M.R., Agostinho, P., Marisco, P.C., Vieira, J.M., Rosa, M.M., Bohnert, C., Rubin, M.A., Morsch, V.M., Spanevello, R., Mazzanti, C.M., 2014. Neuroprotective effect of anthocyanins on acetylcholinesterase activity and attenuation of scopolamine-induced amnesia in rats. *Int. J. Dev. Neurosci.* **33**, 88-97.

Hamodat, H., Cash, M.K., Fisk, J.D., Darvesh, S., 2017. Cholinesterases in normal and alzheimer's disease primary olfactory gyrus. *Neuropathol. Appl. Neurobiol.* https://doi.org/ 10.1111/nan.12423.

He, D.D., Wu, H., Wei, Y., Liu, W., Huang, F., Shi, H.L., Wang, C.H., 2015. Effects of harmine, an acetylcholinesterase inhibitor, on spatial learning and memory of APP/PS1 transgenic mice and scopolamine-induced memory impairment mice. *Eur. J. Pharmacol.* **768,** 96-107.

Jacobson, G.A., Raidal, S., Robson, K., Narkowicz, C., Nichols, D., Haydn Walters, E., 2017. Bronchopulmonary pharmacokinetics of (R)- salbutamol and (S)- salbutamol enantiomers in pulmonary epithelial lining fluid and lung tissue of horses. *Br. J. Clin. Pharmacol.* **83,** 1436-1445.

Joshi, B.S., Newton, M.G., Lee, D.W., Barber, A., Pelletier, S., 1996. Reversal of absolute stereochemistry of the pyrrolo [2, 1-b] quinazoline alkaloids vasicine, vasicinone, vasicinol and vasicinolone. *Tetrahedron: Asymmetry* **7,** 25-28.

Kanamaru, T., Kamimura, N., Yokota, T., Iuchi, K., Nishimaki, K., Takami, S., Akashiba, H., Shitaka, Y., Katsura, K., Kimura, K., Ohta S., 2015. Oxidative stress accelerates amyloid deposition and memory impairment in a double-transgenic mouse model of Alzheimer's disease. *Neurosci. Lett.* **587,** 126-131.

Lam, B., Hollingdrake, E., Kennedy, J.L., Black, S., Masellis, M., 2009. Cholinesterase inhibitors in Alzheimer's disease and Lewy body spectrum disorders: the emerging pharmacogeneticstory. *Hum. Genomics* **4,** 91-106.

Li, S.P., Teng, L., Liu, W., Cheng, X.M., Jiang, B., Wang, Z.T., Wang, C.H., 2016. Interspecies metabolic diversity of harmaline and harmine in *in vitro* 11 mammalian liver microsomes. *Drug Test. Anal*. **9,** 754-768.

Liu, W., Yang, Y.D., Cheng, X.M., Gong, C., Li, S.P., He, D.D., Wang, C.H., 2014. Rapid and sensitive detection of the inhibitive activities of acetyl- and butyryl-cholinesterases inhibitors by UPLC-ESI-MS/MS. *J. Pharm. Biomed. Anal*. **94,** 215-220.

Liu, W., Wang, Y.L., He, D.D., Li, S.P., Zhu, Y.D., Jiang, B., Wang, C.H., 2015a. Antitussive, expectorant, and bronchodilating effects of quinazoline alkaloids (±)-vasicine, deoxyvasicine, and (±)-vasicinone from aerial parts of Peganumharmala L. *Phytomedicine* **22,** 1088-1095.

Liu, W., Shi, X.Y., Yang, Y.D., Cheng, X.M., Liu, Q., Han, H., Wang, Z.T., Wang, C.H., 2015b. *In vitro* and *in vivo* metabolism and inhibitory activities of vasicine, a potent acetylcholinesterase and butyrylcholinesterase inhibitor. *PLoS One* **10,** e0122366.

Liu, W., He, D.D., Zhu, Y.D., Cheng, X.M., Xu, H., Wang, Y.L., Wang, C.H., 2015c. Simultaneous determination of vasicine and its major metabolites in rat plasma by UPLC-MS/MS and its application to *in vivo* pharmacokinetic studies. *RSC Adv*. **5,** 78336-78351.

Liu, W., 2016. Studies on the effects of improving learning and memory, antitussive and bronchodilating of aerial parts of *Peganum harmala* and its active alkaloids [dissertation]. Shanghai: Shanghai University of Traditional Chinese Medicine.

Liu, W., Zhu, Y.D., Wang, Y.W., Qi, S.L., Wang, Y.L., Ma, C., Li, S.P., Jiang, B., Cheng, X.M., Wang, Z.T., Xuan, Z.Y., Wang, C.H., 2017. Anti-amnesic effect of extract and alkaloid fraction from aerial parts of peganum harmala on scopolamine-induced memory deficits in mice. *J. Ethnopharmacol*. **204**, 95-106.

Ma, M., Umemura, T., Mori, Y., Gong, Y.Y., Saijo, Y., Sata, F., Kishi, R., 2005. Influence of genetic polymorphisms of styrene-metabolizing enzymesand smoking habits on levels of urinary metabolites after occupationalexposure to styrene. *Toxicol. Lett*. **160,** 84-91.

Maddi, S., Yamsani, M.R., Seeling A., 2010. Stereoselective plasma protein binding of amlodipine. *Chirality* **22,** 262-266.

Mahindroo, N., Ahmed, Z., Bhagat, A., Bedi, K., Khajuria, R., Kapoor, V., Dhar, K., 2005. Synthesis and structure-activity relationships of vasicine analogues as bronchodilatory agents. *Med. Chem. Res.* **14,** 347-368.

Miners, J.O., Bowalgaha, K., Elliot, D.J., Baranczewski, P., Knights, K., 2011. Characterization of niflumic acid as a selective inhibitor of human liver microsomal UDP-glucuronosyltransferase 1A9: application to the reaction phenotyping of acetaminophen glucuronidation. *Drug Metab. Dispos.* **39,** 644-652.

Mukherjee, P.K., Kumar, V., Mal, M., Houghton, P., 2007. Acetylcholinesterase inhibitors from plants. *Cheminform* **14,** 289-300.

Nachon, F., Carletti, E., Ronco, C., Trovaslet, M., Nicolet, Y., Jean, L., Renard, P., 2013. Crystal structures of human cholinesterases in complex with huprine W and tacrine: elements of specificity for anti-Alzheimer's drugs targeting acetyl-and butyryl-cholinesterase. *Biochem. J.* **453,** 393-399.

Obach, R.S., Baxter, J.G., Liston, T.E., Silber, B., Jones, B., Macintyre F., Wastall, P., 1997. The prediction of human pharmacokinetic parameters from preclinical and *in vitro* metabolism data. *J. Pharmacol. Exp. Ther.* **283,** 46-58.

Pa, R., Mathew, L., 2012. Antimicrobial activity of leaf extracts of Justiciaadhatoda L. in comparison with vasicine. *Asian Pac. J. Trop. Biomed.* **2,** 1556-1560.

Pistolozzi, M., Du, H., Wei, H., Tan, W., 2015. Stereoselectiveinhibition of human butyrylcholinesterase by the enantiomers of bambuterol and their Intermediates. *Drug Metab. Dispos.* **43,** 344-352.

Raungrut, P., Uchaipichat, V., Elliot, D.J., Janchawee, B., Somogyi, A., Miners, J., 2010. *In vitro-in vivo* extrapolation predicts drug-drug interactions arising from inhibition of codeine glucuronidation by dextropropoxyphene, fluconazole, ketoconazole, and methadone in humans. *J. Pharmacol. Exp. Ther.* **334,** 609-18.

Reist, M., Carrupt, P.A., Francotte, E., Testa, B., 1998. Chiral inversion and hydrolysisof thalidomide: mechanisms and catalysis by bases and serum albumin, and chiral stability of teratogenic metabolites. *Chem. Res. Toxicol.* **11,** 1521–1528.

Rosenberry, T.L., Sonoda, L.K., Dekat, S.E., Cusack, B., Johnson, J., 2008. Analysis of the reaction of carbachol with acetylcholinesterase with thioflavin T as a coupled fluorescence reporter. *Biochemistry* **47,** 13056-13063.

SFDA, Drug registration administration office [EB/OL]. 2007. http://www.sda.gov.cn/WS01/CL0205/ 15220.html.

Shen, Q., Wang, L., Zhou, H., Jiang, H., Yu, L., Zeng, S., 2013. Stereoselective binding of chiral drugs to plasma proteins. *Acta Pharmacol. Sin.* **34:** 998-1006.

Smith S.W., 2009. Chiral toxicology: it's the same thing… only different. *Toxicol. Sci.* **110.** 4-30.

Srinivasarao, D., Jayarrajl, I.A., Jayraajz, R., Prabhal, M., 2006. A study on Antioxidant and Anti-inflammatory activity of Vasicine against lung damage in rats. *Indian Allergy Asthma Immunol.* **20,** 1-7.

Tao, L., Xie, J., Wang, Y., Wang, S., Wu, S., Wang, Q., Ding, H., 2014. Protective effects of aloe-emodin on scopolamine-induced memory impairment in mice and H2O2-induced cytotoxicity in PC12 cells. *Bioorg. Med. Chem. Lett.* **24,** 5385-5389.

Uchaipichat, V., Mackenzie, P.I., Elliot, D.J., Miners, J., 2006. Selectivity of substrate (trifluoperazine) and inhibitor (amitriptyline, androsterone, canrenoic acid, hecogenin, phenylbutazone, quinidine, quinine, and sulfinpyrazone) "probes" for human UDP-glucuronosyltransferases. *Drug Metab. Dispos.* **34,** 449-456.

Uchaipichat, V., Mackenzie, P., Guo, X., Gardner-Stephen, D., Galetin, A., Houston, J., Miners, J., 2004. Human UDP-glucuronosyltransferases: isoform selectivity and kinetics of 4-methylumbelliferone and 1-naphthol glucuronidation, effects of organic solvents, and inhibition by diclofenac and probenecid. *Drug Metab. Dispos.* **32,** 413-423.

Xian, Y., Ip, S., Mao, Q., Su, Z., Chen, J., Lai, X., Lin, Z., 2015. Honokiol improves learning and memory impairments induced by scopolamine in mice. *Eur. J. Pharmacol.* **760,** 88-95.

Zhang, D., Chando, T.J., Everett, D.W., Patten, C., Dehal, S., Humphreys, W., 2005. *In vitro* inhibition of UDP glucuronosyltransferases by atazanavir and other HIV protease inhibitors and the relationship of this property to *in vivo* bilirubin glucuronidation. *Drug Metab. Dispos.* **33,** 1729-1739.

Zhang, K., Tang, C., Rashed, M., Cui, D., Tombret, F., Botte, H., Lepage, F., Levy, R.H., Baillie, T.A., 1994. Metabolic chiral inversion of stiripentol in the rat. I. Mechanistic studies. *Drug Metab. Dispos.* **22,** 544–553.

Zhao, T., Ding, K.M., Zhang, L., Cheng, X.M., Wang, C.H., Wang, Z.T., 2013. Acetylcholinesterase and Butyrylcholinesterase Inhibitory Activities of β-Carboline and Quinoline Alkaloids Derivatives from the Plants of Genus Peganum. *J. Chem.* http://dx.doi.org/10.1155/2013/717232.

Figure legends

Fig. 1. Identification of UGTs responsible for glucuronidation of *rac*-VAS, *l*-VAS and *d*-VAS in HLM by specific inhibitory test. A-E: formation of glucuronidation metabolites *d*-VASG and *l*-VASG by specific inhibitory test after incubation with 250 μM *rac*-VAS (A and B), *l*-VAS (C) and *d*-VAS (D and E) in HLM for 60 min. The selective inhibitors were used atazanavir (UGT1A1), hecogenin (UGT1A4) and fluconazole (UGT2B7) at individual concentrations of 1, 10 and100 μM; niflumic acid (UGT1A9) at concentrations of 10, 100 and 500 μM; phenylbutazone (UGT1As) and diclofenac (UGT2B15) at concentrations of100, 500 and 1000 μM.

Fig. 2. Identification of UGTs responsible for glucuronidation of *rac*-VAS, *l*-VAS and *d*-VAS by rhUGTs assay. A-C: formation of glucuronidation metabolites *d*-VASG and *l*-VASG by rhUGTs after incubation with 250 μM *rac*-VAS (A), *l*-VAS (B) and *d*-VAS (C) for 60 min

Fig. 3. The enzyme kinetics of *d*-VASG and *l*-VASG generation in HLM after incubation with *rac*-VAS (30-500 μM) (A and B), *l*-VAS (15-250 μM) (C) and *d*-VAS (15-250 μM) (D and E) for 60 min

Fig. 4. Enzyme kinetics of *rac*-VAS (30-500 μM), *l*-VAS (15-250 μM) and *d*-VAS (15-250 μM) after incubation with rhUGTs for 60 min. A to F: the enzyme kinetics of *d*-VASG and *l*-VASG generation in rhUGT1A9 and 2B15 after incubation with *rac*-VAS (A, B and E), *l*-VAS (C and F) and *d*-VAS (D) for 60 min.

Fig. 5. Plasma concentration–time profiles of *d*-VAS, *l*-VAS and their glucuronidation metabolites in rats plasma after intravenously and oral administration of *d*-VAS or *l*-VAS: (A) The plasma concentration–time profiles of *d*-VAS and *l*-VAS after intravenous dose of 1 $mg \cdot kg^{-1}$ *d*-VAS and *l*-VAS, respectively. (B) The plasma concentration–time profiles of *d*-VAS and *l*-VAS after oral dose of 7.5 $mg \cdot kg^{-1}$ *d*-VAS and *l*-VAS, respectively. (C) The plasma concentration–time profiles of *d*-VASG and *l*-VASG after intravenous dose of 1 $mg \cdot kg^{-1}$ *l*-VAS. (D) The plasma concentration–time profiles of *d*-VASG and *l*-VASG after intravenous dose of 1 $mg \cdot kg^{-1}$ *d*-VAS. (E) The plasma concentration–time profiles of *d*-VASG and *l*-VASG after oral dose of 7.5 $mg \cdot kg^{-1}$ *l*-VAS. (F) The plasma concentration–time profiles of *d*-VASG and *l*-VASG after oral dose of 7.5 $mg \cdot kg^{-1}$ *d*-VAS. Intravenous administration group was shown “black” line, oral administration group was shown “red”

line. Solid symbols represent administration of *d*-VAS, and empty symbols represent administration of *l*-VAS.

Fig. 6. The IC_{50} of *d*-VAS, *l*-VAS, and mistures of *d*-VAS and *l*-VAS with different ratios on AChE and BChE *in vitro*.

Fig. 7. Molecular docking of *d*-VAS and *l*-VAS with hAChE and hBChE. A: The 3D interaction map of *d*-VAS and hAChE; B: The 2D interaction-map of *d*-VAS and hAChE; C: The 3D interaction map of *l*-VAS and hAChE; D: The 2D interaction-map of *l*-VAS and hAChE; E: The 3D interaction map of *d*-VAS and hBChE; F: The 2D interaction-map of *d*-VAS and hBChE; G: The 3D interaction map of *l*-VAS and hBChE; H: The 2D interaction-map of *l*-VAS and hBChE.

Fig. 8. Effects of *rac*-VAS, *l*-VAS and *d*-VAS on scopolamine-induced memory-impaired mice. The dosages of *rac*-VAS, *l*-VAS, *d*-VAS and donepezil (15, 15, 15, and 3 $mg \cdot kg^{-1} \cdot day^{-1}$, respectively) were administered by oral gavage two weeks prior to the training for Morris water maze test. Memory impairment was induced by scopolamine (1 $mg \cdot kg^{-1}$, i.p.). A: Escape latency of mice in hidden platform tests for five consecutive days; B: Path length of mice in hidden platform tests for five consecutive days; C: Frequency of mice passing through the platform location; D: Swimming tracks of mice in water tank. The green circle indicated the hidden platform location, and red curves represented the movement tracks. The error bar (SD) for data points in A and B were not shown in order to clearly discriminate the difference among treatments. N=8/group. *, p <0.05; ** p <0.01; ***, p <0.001, *versus* scopolamine-treated group. $^{\#}$, p <0.05; $^{\#\#}$, p <0.01, *versus* control group.

Fig. 9. Effects of *rac*-VAS, *l*-VAS and *d*-VAS on the content of ACh and Ch and the levels of AChE and ChAT in the cerebral cortex and hippocampus of scopolamine-induced memory-impaired mice. The content of ACh (A) and Ch (B) on cerebral cortex; the activities of AChE on cerebralcortex (C) and hippocampus (D) and ChAT on cerebral cortex (E). Western blots and gray intensity analysis of AChE and ChAT on cerebral cortex (F-H) and hippocampus (I-K). 1, control group; 2, model group; 3, positive group; 4, *rac*-VAS group; 5, *l*-VAS group; 6, *d*-VAS group. Data were expressed as the means ±SD (n=10). *, p<0.05; **, p<0.01; ***, p<0.001 *versus* scopolamine-treated group. $^{\#}$, p<0.05; $^{\#\#}$, p <0.01; $^{\#\#\#}$, p <0.001, *versus* control group.

Table 1. Enzyme kinetic parameters for VAS to VASG in rhUGTs system (mean ± SD, n = 3)

Groups	rhUGT enzymes	Metabolites	K_m	V_m	CL_{int}
			μM	pmol·min^{-1}·mg^{-1} protein	μL·min^{-1}·mg^{-1} protein
rac-VAS	1A9	*d*-VASG	163.95±21.28	0.53±0.07	3.21±0.01
rac-VAS	1A9	*l*-VASG	338.05±31.33	0.40±0.09	1.17±0.16
rac-VAS	2B15	*l*-VASG	563.60±53.60	2.01±0.004	3.59±0.33
d-VAS	1A9	*d*-VASG	171.55±12.94	0.40±0.05	2.29±0.12
l-VAS	1A9	*l*-VASG	316.20±80.89	0.84±0.08	2.71±0.45
l-VAS	2B15	*l*-VASG	531.50±44.55	1.72±0.52	3.21±0.70

$CL_{int}=V_{max}/K_m$

Table 2. Pharmacokinetics parameters of *d*-VAS and *l*-VAS and its metabolites *d*-VASG and *l*-VASG in rats after intravenous administration of 1 mg·kg^{-1} *d*-VAS and *l*-VAS (mean ± SD, n = 8)

Pharmacokinetics parameters	*l*-VAS group			*d*-VAS group		
	VAS	*d*-VASG	*l*-VASG	VAS	*d*-VASG	*l*-VASG
k_d (min^{-1})	0.02±0.01	0.02±0.01	0.02±0.01	0.02±0.01	0.04±0.04	0.03±0.02
$t_{1/2kd}$ (min)	57.66±41.39	47.70±32.66	56.30±43.69	45.99±29.48	39.28±38.46	22.81±10.08 **
k_a (min^{-1})	0.02±0.01	0.03±0.02	0.05±0.01	0.03±0.01	0.05±0.03	0.05±0.02
$t_{1/2ka}$ (min)	62.25±42.24	33.32±24.12	16.65±4.70	34.76±29.67 *	16.68±7.52*	14.83±4.26
k_e (min^{-1})	0.01±0.01	0.001±0.001	0.01±0.004	0.004±0.001	0.01±0.004	0.02±0.02
$t_{1/2ke}$ (min)	78.46±31.32	2843.15±1953.21	138.90±63.41	202.48±73.50***	94.91±75.23 ***	37.22±16.09***
C_{max} (μg·mL^{-1})	0.16±0.02	2.59±0.69	97.27±54.80	0.19±0.014**	4.86±1.75 ***	8.12±4.19 ***
T_{max} (min)	2.00±0	37.50±14.58	30.00±7.07	2.00±0	53.33±10.90 *	38.33±13.23
$AUC_{(0-t)}$ (μg·min^{-1}·mL^{-1})	15.98±4.96	0.57±0.08	11.96±6.85	21.19±8.61 *	1.19±0.78 **	1.32±0.86 ***
$AUC_{(0-\infty)}$ (μg·min^{-1}·mL^{-1})	16.01±4.94	2.36±1.20	12.37±6.29	21.87±8.68*	1.24±0.78 *	1.49±0.88 ***
MRT (min)	68.08±42.44	3090.27±2786.61	109.48±16.85	148.19±32.12 ***	115.97±78.54 ***	60.07±42.47***
V_d/F(mL·kg^{-1})	6557.90±4252.54	1148097.65±464138.56	11345.20±6334.89	14652.03±6742.82 **	119858.22±112474.88 ***	170790.10±167477.13**
CL/F(mL·min^{-1}·kg^{-1})	57.86±25.60	564.10±357.23	56.12±20.27	50.84±14.44	873.40±551.00**	763.63±416.87***

All the pharmacokinetic data were processed using the noncompartmental pharmacokinetics data analysis. "*: $p < 0.05$, **: $p < 0.01$ and ***: $p < 0.001$ versus l-VAS group".

Table 3. Pharmacokinetics parameters of *d*-VAS and *l*-VAS and its metabolites *d*-VASG and *l*-VASG in rats after oral administration of 7.5 mg·kg^{-1} *d*-VAS and *l*-VAS (mean ±SD, n = 8)

Pharmacokinetics parameters	*l*-VAS group			*d*-VAS group		
	VAS	*d*-VASG	*l*-VASG	VAS	*d*-VASG	*l*-VASG
k_d (min^{-1})	0.03±0.01	0.04±0.01	0.03±0.02	0.02±0.02	0.02±0.01	0.02±0.02
$t_{1/2kd}$ (min)	21.40±6.71	21.04±6.71	57.10±64.89	30.09±14.58	52.62±28.89 *	72.90±60.73
k_a (min^{-1})	0.04±0.01	0.04±0.01	0.03±0.02	0.03±0.01	0.03±0.02	0.04±0.03
$t_{1/2ka}$ (min)	20.38±4.88	19.63±4.50	51.75±84.76	25.78±12.51	26. 70±15.98	24.45±17.30
k_e (min^{-1})	0.005±0.001	0.003±0.002	0.005±0.002	0.006±0.002	0.057±0.002	0.006±0.003
$t_{1/2ke}$ (min)	115.32±31.06	203.75±55.14	183.02±85.71	151.54±38.56*	104.12±21.78 **	96.36±31.73 *
C_{max}(μg·mL^{-1})	0.54±0.08	0.02±0.01	1.16±0.20	0.91±0.21 ***	0.03±0.01**	0.04±0.01 ***
T_{max} (min)	45.00±0	38.57±8.02	40.71±11.34	48.00±6.71	46.88±16.89	45.00±11.34
$AUC_{(0-t)}$ (μg·min^{-1}·mL^{-1})	78.81±10.29	3.32±1.04	158.53±33.97	127.97±21.95***	5.80±1.38 **	6.74±1.45 ***
$AUC_{(0-\infty)}$ (μg·min^{-1}·mL^{-1})	79.68±10.39	3.47±1.04	160.59±34.11	128.72±21.82 ***	5.86±1.41 **	7.01±1.83 ***
MRT (min)	128.67±19.71	187.59±79.93	136.94±21.57	129.97±16.18	150.31±16.52	180.92±82.25
V_d/F(mL·kg^{-1})	20816.68±5418.64	1180317.21±93493.61	12755.56±9344.33	9932.63±3333.25**	265009.077±91445.98 **	259821.93±222120.83***
CL/F(mL·min^{-1}·kg^{-1})	95.67±13.92	2710.66±441.77	49.41±10.88	59.44±8.67***	1347.16±324.25 ***	1126.71±257.58 ***

All the pharmacokinetic data were processed using the noncompartmental pharmacokinetics data analysis. "*: $p < 0.05$, **: $p < 0.01$ and ***: $p < 0.001$ versus l-VAS group".

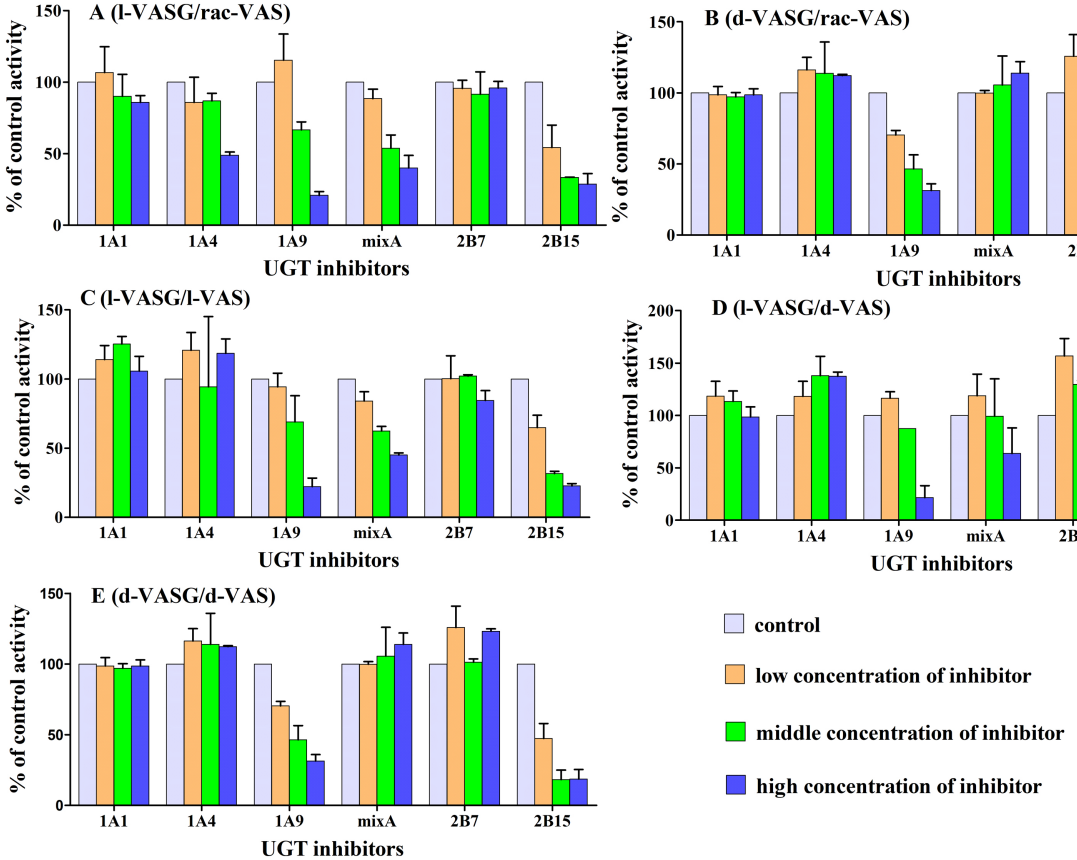
A (l-VASG/rac-VAS)
B (d-VASG/rac-VAS)
C (l-VASG/l-VAS)
D (l-VASG/d-VAS)
E (d-VASG/d-VAS)
% of control activity
UGT inhibitors
1A1
1A4
1A9
mixA
2B7
2B15
control
low concentration of inhibitor
middle concentration of inhibitor
high concentration of inhibitor

Figure 1

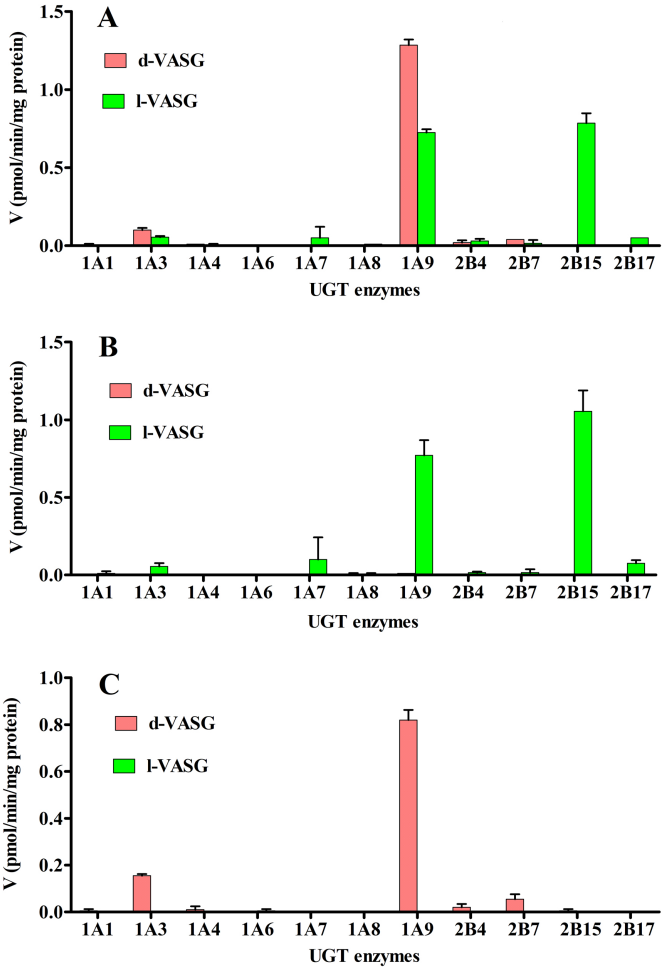
A
d-VASG
l-VASG
V (pmol/min/mg protein)
1.5
1.0
0.5
0.0
1A1 1A3 1A4 1A6 1A7 1A8 1A9 2B4 2B7 2B15 2B17
UGT enzymes
B
d-VASG
l-VASG
V (pmol/min/mg protein)
1.5
1.0
0.5
0.0
1A1 1A3 1A4 1A6 1A7 1A8 1A9 2B4 2B7 2B15 2B17
UGT enzymes
C
d-VASG
l-VASG
V (pmol/min/mg protein)
1.0
0.8
0.6
0.4
0.2
0.0
1A1 1A3 1A4 1A6 1A7 1A8 1A9 2B4 2B7 2B15 2B17
UGT enzymes

Figure 2

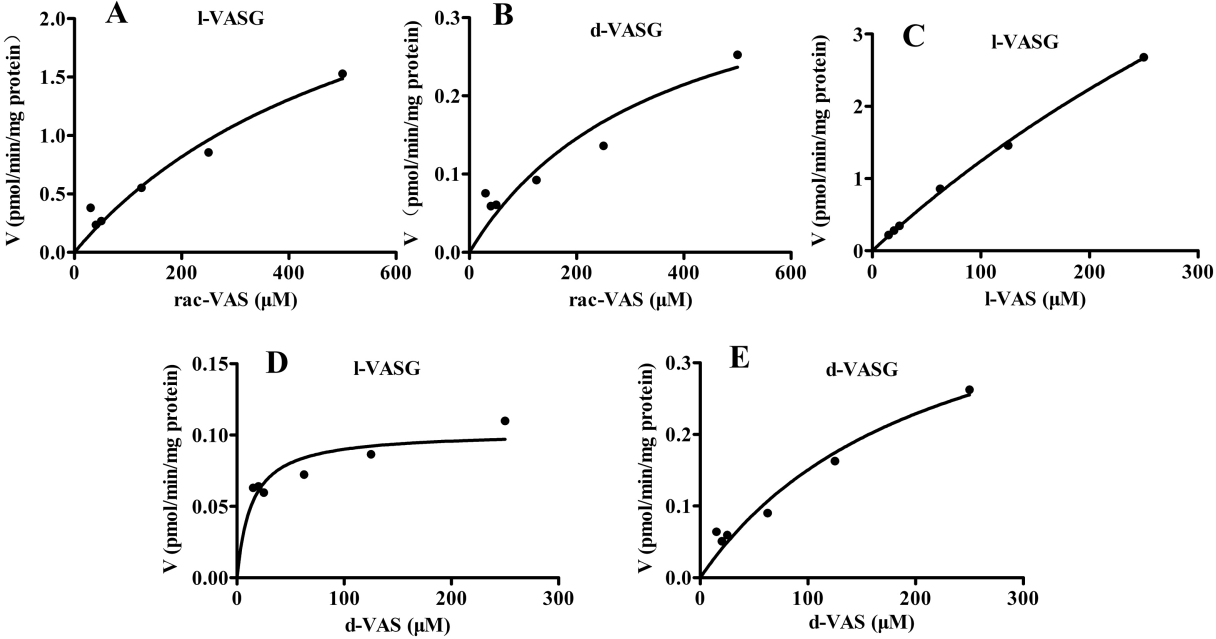
A
l-VASG
V (pmol/min/mg protein)
rac-VAS (μM)
B
d-VASG
V (pmol/min/mg protein)
rac-VAS (μM)
C
l-VASG
V (pmol/min/mg protein)
l-VAS (μM)
D
l-VASG
V (pmol/min/mg protein)
d-VAS (μM)
E
d-VASG
V (pmol/min/mg protein)
d-VAS (μM)

Figure 3

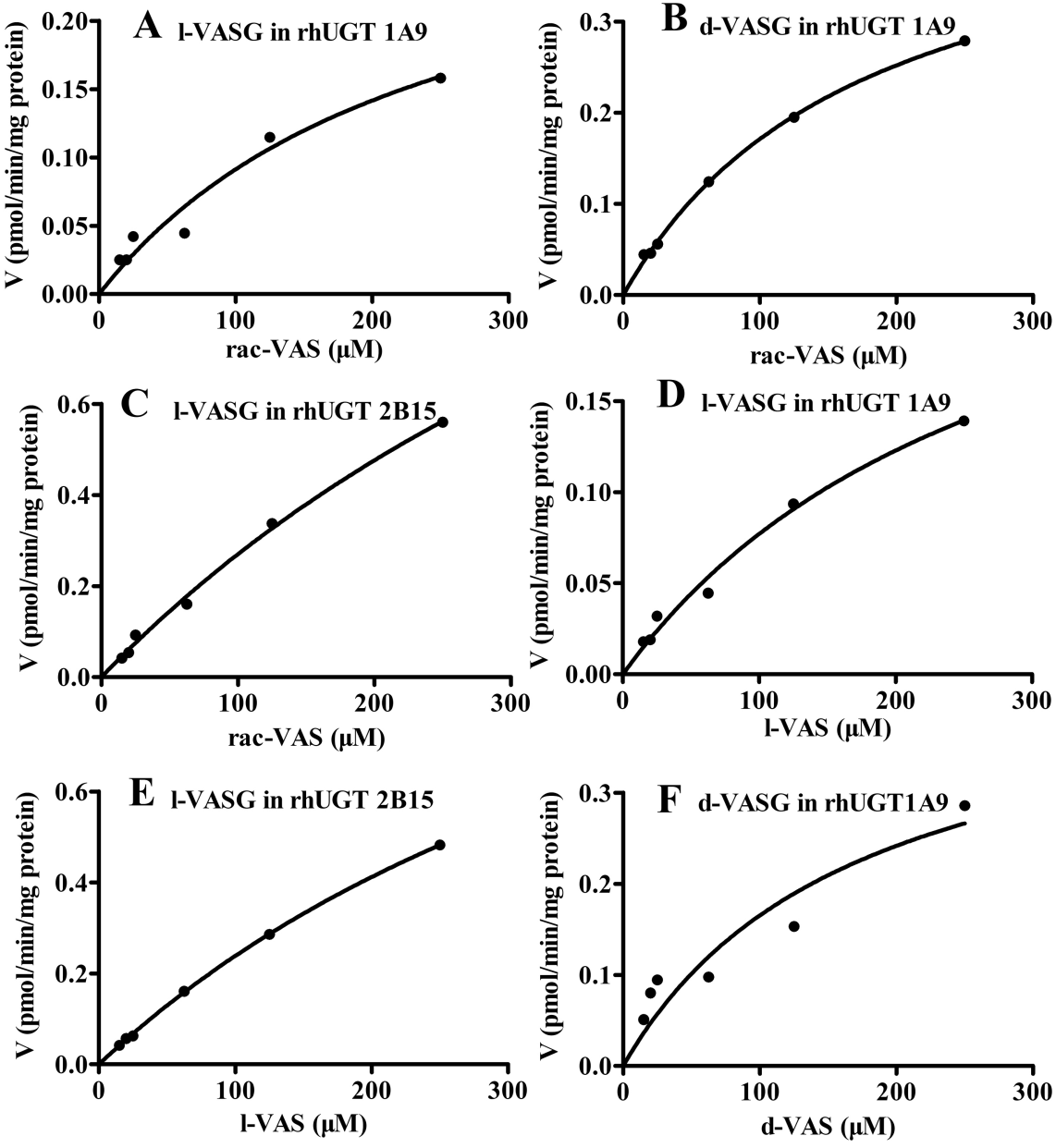
A l-VASG in rhUGT 1A9
V (pmol/min/mg protein)
rac-VAS (μM)
B d-VASG in rhUGT 1A9
V (pmol/min/mg protein)
rac-VAS (μM)
C l-VASG in rhUGT 2B15
V (pmol/min/mg protein)
rac-VAS (μM)
D l-VASG in rhUGT 1A9
V (pmol/min/mg protein)
l-VAS (μM)
E l-VASG in rhUGT 2B15
V (pmol/min/mg protein)
l-VAS (μM)
F d-VASG in rhUGT1A9
V (pmol/min/mg protein)
d-VAS (μM)

Figure 4

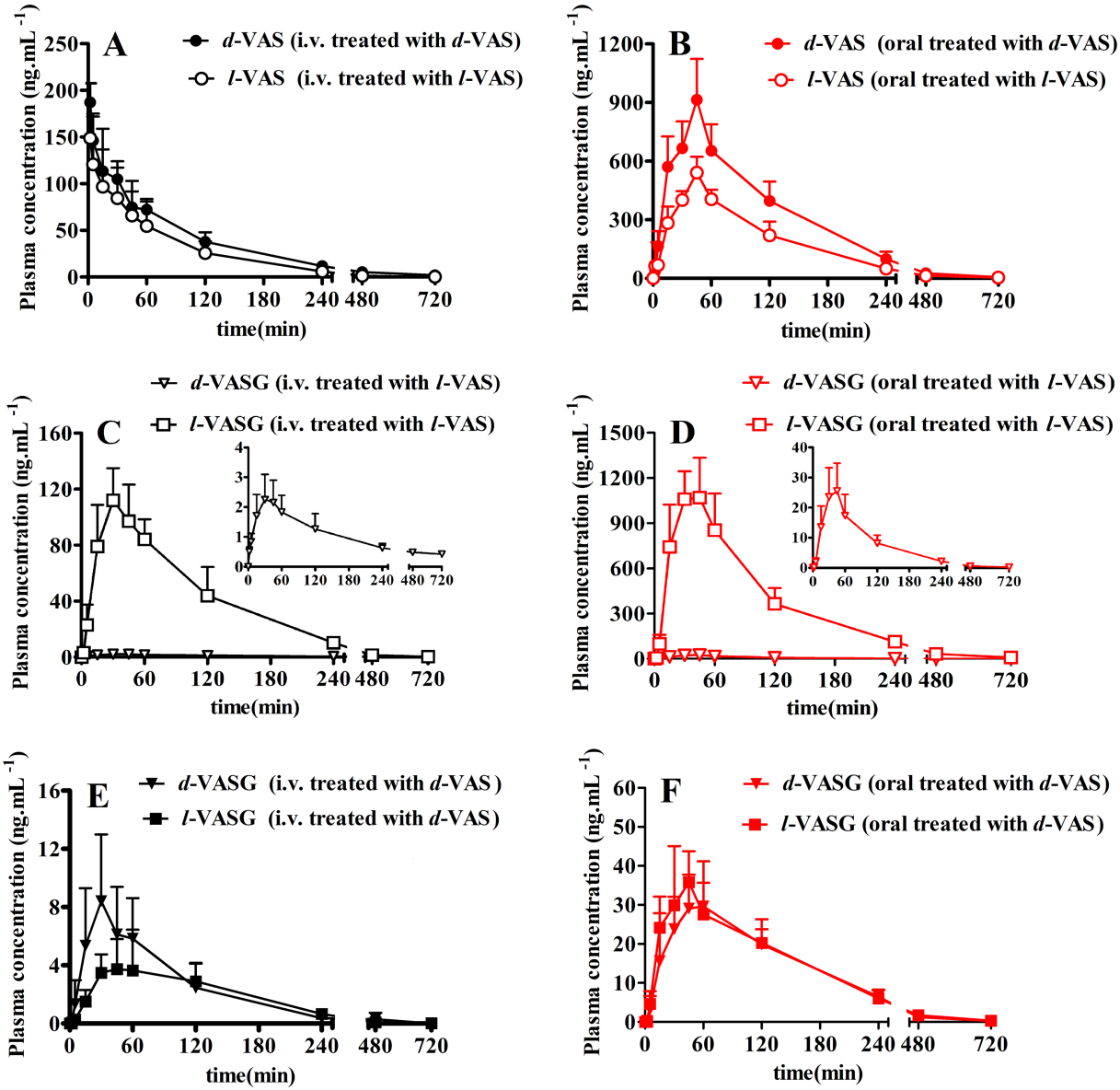
A
d-VAS (i.v. treated with d-VAS)
l-VAS (i.v. treated with l-VAS)
Plasma concentration (ng.mL -1)
time(min)
B
d-VAS (oral treated with d-VAS)
l-VAS (oral treated with l-VAS)
Plasma concentration (ng.mL -1)
time(min)
C
d-VASG (i.v. treated with l-VAS)
l-VASG (i.v. treated with l-VAS)
Plasma concentration (ng.mL -1)
time(min)
D
d-VASG (oral treated with l-VAS)
l-VASG (oral treated with l-VAS)
Plasma concentration (ng.mL -1)
time(min)
E
d-VASG (i.v. treated with d-VAS)
l-VASG (i.v. treated with d-VAS)
Plasma concentration (ng.mL -1)
time(min)
F
d-VASG (oral treated with d-VAS)
l-VASG (oral treated with d-VAS)
Plasma concentration (ng.mL -1)
time(min)

Figure 5

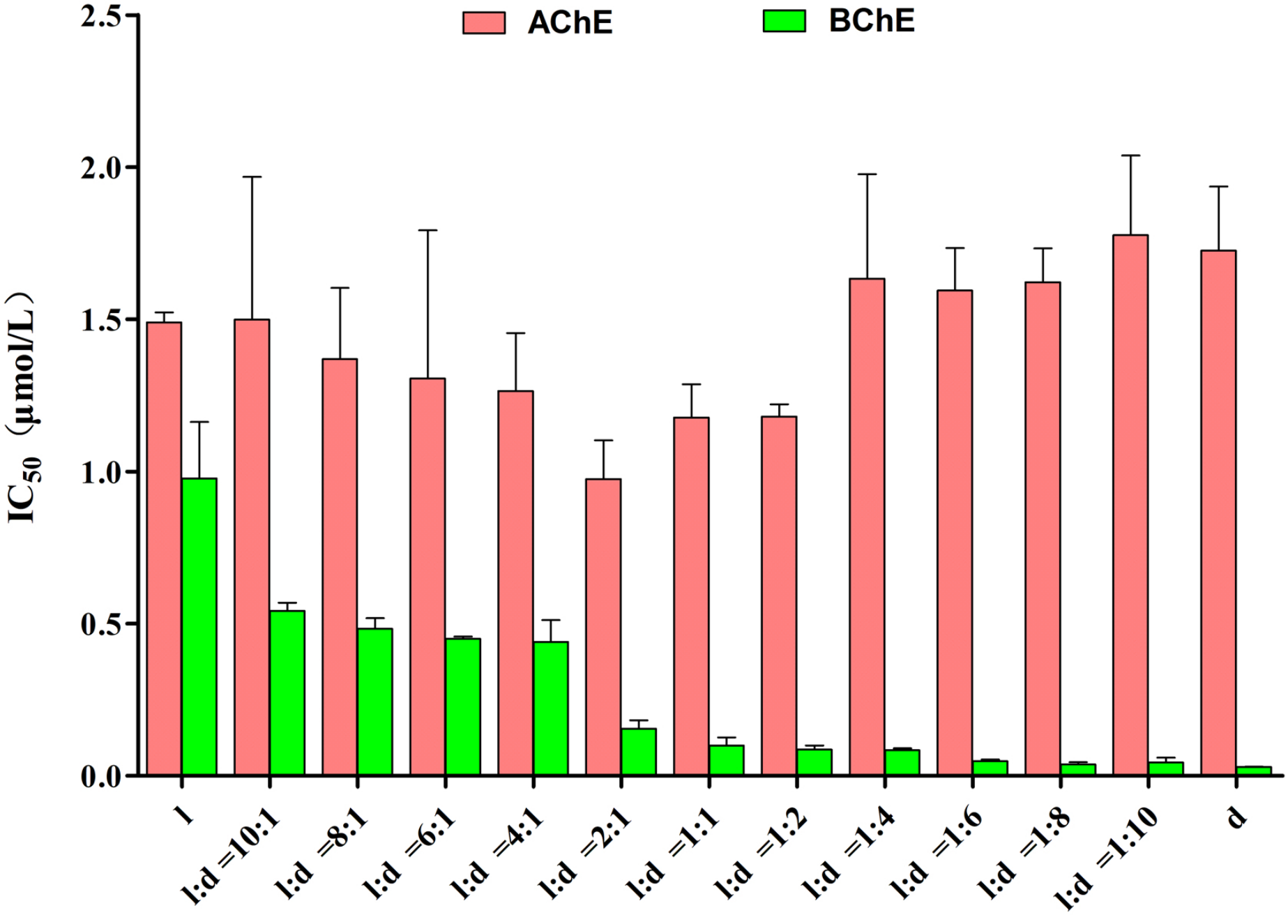
AChE
BChE
2.5
2.0
1.5
1.0
0.5
0.0
IC50 （μmol/L）
1
1:d =10:1
1:d =8:1
1:d =6:1
1:d =4:1
1:d =2:1
1:d =1:1
1:d =1:2
1:d =1:4
1:d =1:6
1:d =1:8
1:d =1:10
d

Figure 6

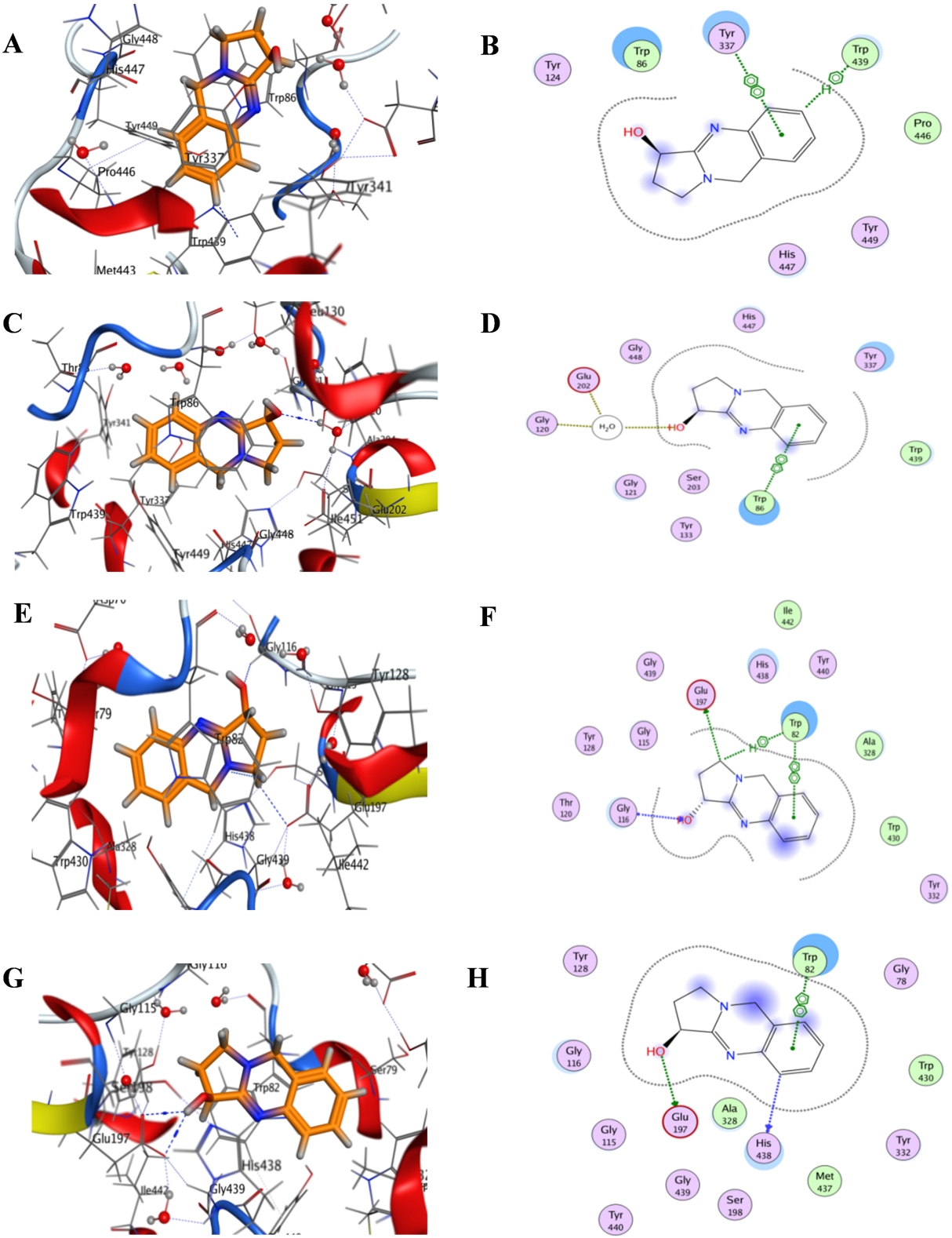
A
Gly448
His447
Trp86
Tyr449
Tyr337
Pro446
Tyr341
Trp439
Met443
B
Tyr 337
Trp 86
Tyr 124
Trp 439
H
HO
N
N
Pro 446
Tyr 449
His 447
C
Trp86
Tyr341
Trp439
Tyr337
Ile451
Glu202
Gly448
Tyr449
D
His 447
Gly 448
Tyr 337
Glu 202
Gly 120
H2O
HO
N
N
Trp 439
Gly 121
Ser 203
Trp 86
Tyr 133
E
Gly116
Tyr128
Trp82
Glu197
His438
Gly439
Ile442
Trp430
F
Ile 442
Gly 439
His 438
Tyr 440
Glu 197
Trp 82
Tyr 128
Gly 115
Ala 328
H
HO
N
N
Thr 120
Gly 116
Trp 430
Tyr 332
G
Gly115
Tyr128
Ser79
Trp82
Glu197
His438
Ile442
Gly439
H
Tyr 128
Trp 82
Gly 78
Gly 116
HO
N
N
Trp 430
Glu 197
Ala 328
Gly 115
His 438
Tyr 332
Gly 439
Met 437
Ser 198
Tyr 440

Figure 7

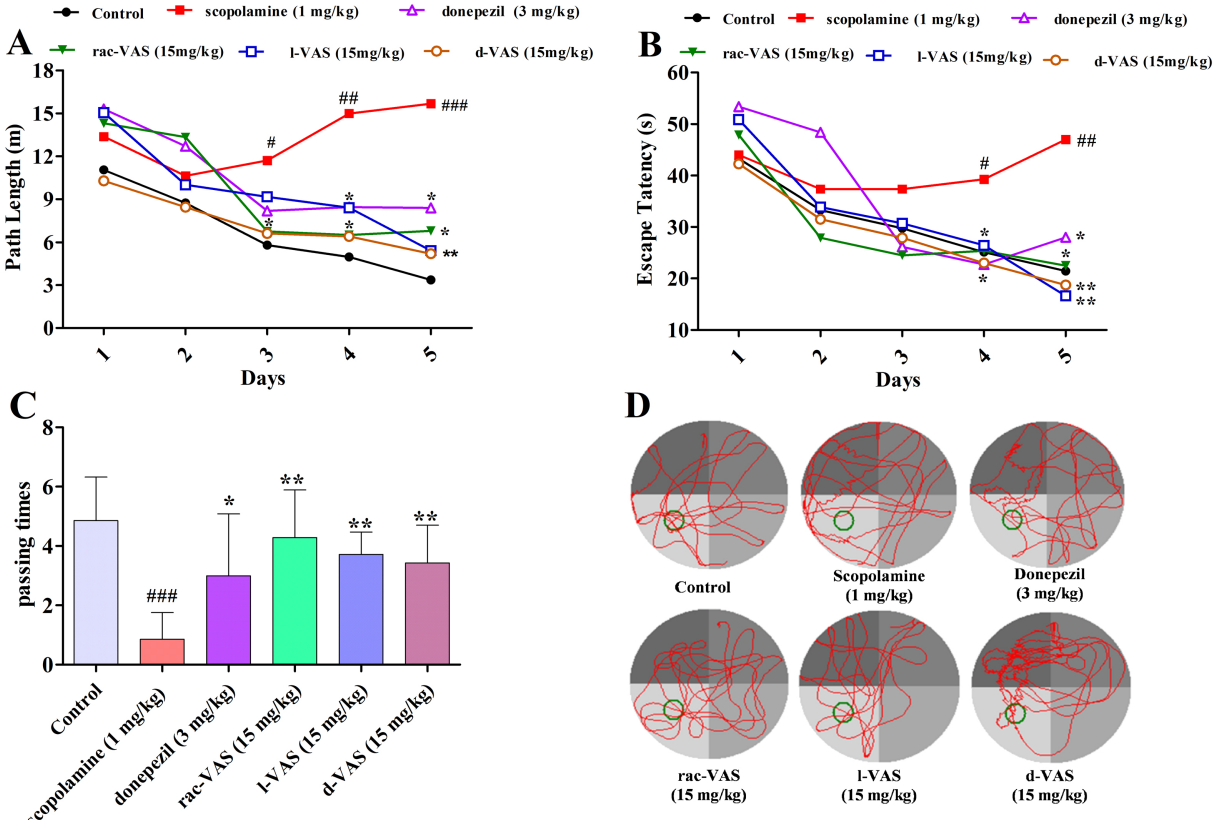
A
Control
scopolamine (1 mg/kg)
donepezil (3 mg/kg)
rac-VAS (15mg/kg)
l-VAS (15mg/kg)
d-VAS (15mg/kg)
Path Length (m)
Days
B
Escape Tatency (s)
Days
C
passing times
Control
scopolamine (1 mg/kg)
donepezil (3 mg/kg)
rac-VAS (15 mg/kg)
l-VAS (15 mg/kg)
d-VAS (15 mg/kg)
D
Control
Scopolamine (1 mg/kg)
Donepezil (3 mg/kg)
rac-VAS (15 mg/kg)
l-VAS (15 mg/kg)
d-VAS (15 mg/kg)

Figure 8

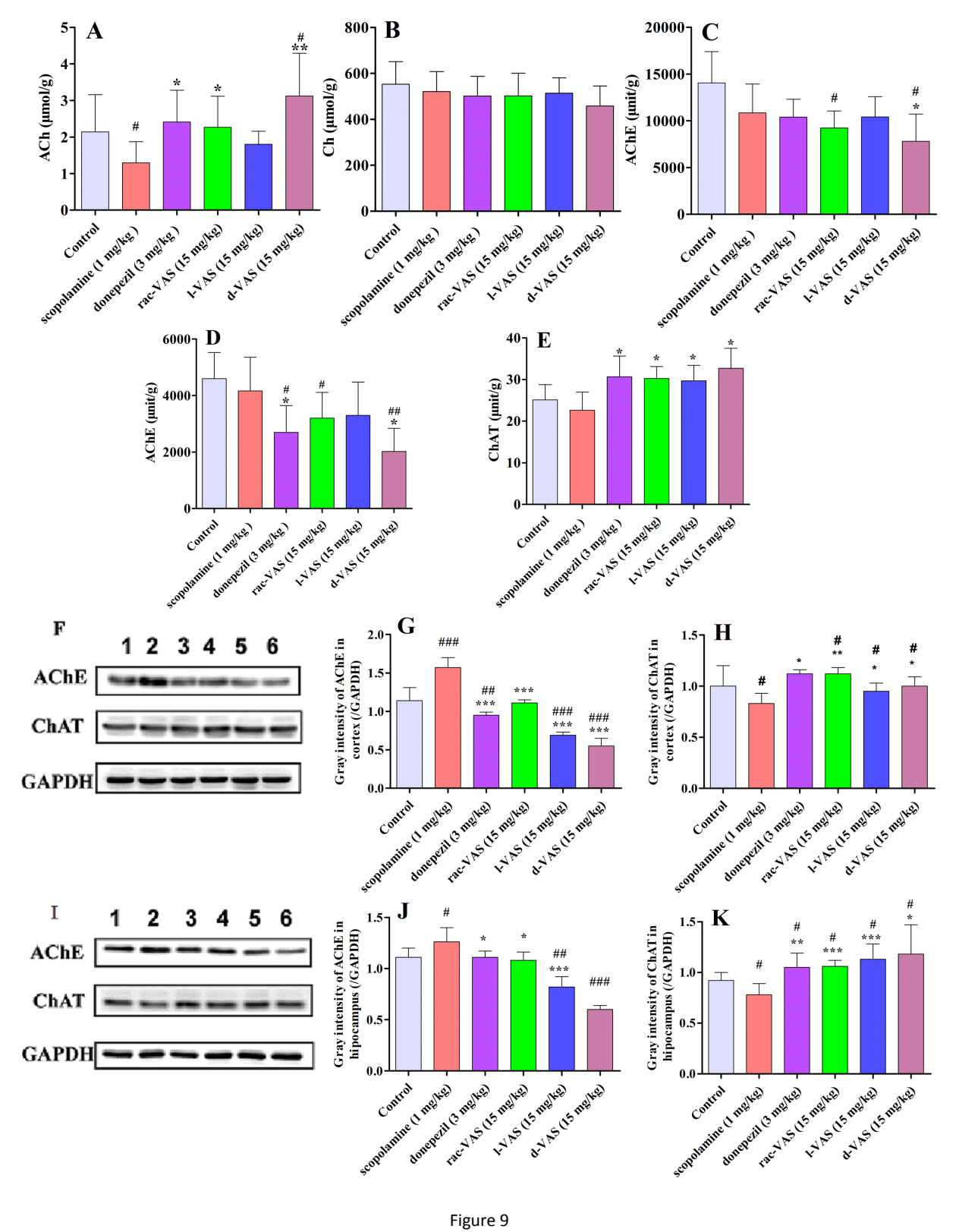
A
ACh (μmol/g)
B
Ch (μmol/g)
C
AChE (μnit/g)
D
AChE (μnit/g)
E
ChAT (μnit/g)
Control
scopolamine (1 mg/kg)
donepezil (3 mg/kg)
rac-VAS (15 mg/kg)
l-VAS (15 mg/kg)
d-VAS (15 mg/kg)
F
1 2 3 4 5 6
AChE
ChAT
GAPDH
G
Gray intensity of AChE in cortex (/GAPDH)
H
Gray intensity of ChAT in cortex (/GAPDH)
I
1 2 3 4 5 6
AChE
ChAT
GAPDH
J
Gray intensity of AChE in hipocampus (/GAPDH)
K
Gray intensity of ChAT in hipocampus (/GAPDH)

Figure 9